AN ABSTRACT OF THE THESIS OF

JOHN LUDWIG MORACK (Name) for the DOCTOR OF PHILOSOPHY (Degree)

in PHYSICS (Major) presented on July 31, 1963 (Date)

Title: MEASURED LIFETIMES FOR THE FIRST EXCITED J = 1 ($^3P_1$) LEVEL IN ARGON AND KRYPTON

Redacted for Privacy

Abstract approved C. E. Fairchild

The first excited multiplet in argon and krypton consists of four levels. Two of these levels, the $^3P_2$ and $^3P_0$ levels, are metastable, while the $^3P_1$ and $^1P_1$ levels decay to the $^1S_0$ ground state by an allowed transition. In the case of pure Russel-Saunders coupling, the transition from the $^3P_1$ level to the ground state is forbidden. However, in both argon and krypton the spin-orbit interaction mixes the $^3P_1$ and $^1P_1$ levels, thus allowing the $^3P_1$ level to decay to the ground state. A measurement of these lifetimes serves as a valuable test of the approximations which have been used in the calculation of wave functions for the $^3P_1$ and $^1P_1$ levels.

The principal result of the present work is the measurement of the natural lifetimes for the first excited J = 1 ($^3P_1$) level in both argon and krypton. This is the first lifetime measurement for a resonance transition in argon and the first direct lifetime measurement

for the $(4p^5 5s)\ ^3P_1$ level in krypton. The experiment in krypton, besides giving an independent determination of this lifetime, was used to investigate resonance trapping. To the author's best knowledge, these measurements for krypton are the first to be interpreted in terms of the recent theory of resonance trapping developed by D'yakonov and Perel'.

The method chosen for these studies is a modified delayed coincidence method. The atomic excitation is produced by bombarding a gas sample with a pulsed beam of electrons. For a given pulse of electrons, the light output from the gas will increase until the excitation is terminated, and then decay exponentially. At some delay time after the excitation is terminated, the light detector is gated to sample the emitted light for a time interval Δt. A Bendix Model M308 magnetic electron multiplier was used as a light detector; the anode section of this photomultiplier was modified to a dual anode configuration in order to sample the light emitted by the gas for time intervals as short as a few nanoseconds. The details of this modification are discussed, and the response of the detector to an exponentially decaying input signal is investigated. It is shown that for the exponential decay, the detector output is proportional to the light intensity at the beginning of the sampling interval. The detector output is then amplified and averaged over many decays, allowing the decay curve to be reconstructed by varying the delay time between the turnoff of the

excitation and the sampling of the emitted light in discrete steps.

All of the resonance transitions in the noble gases lie in the extreme ultraviolet. The transition from the $^3P_1$ and $^1P_1$ levels to the ground state in argon are at 1067 Å and 1048 Å respectively. It was found that a lithium fluoride window between the excitation region and the light detector eliminated any signal from the 1048 Å transition. The gas was excited by an electron gun consisting of the control grid and indirectly heated cathode structure of a 6SJ7 tube. The energy of the bombarding electrons was kept below the threshold for excitation of the $(3p)^5 4p$ levels in order to eliminate cascade contributions to the observed decays. The argon was let into the four liter excitation chamber through a flow system, and the decay of the $^3P_1$ level was investigated at pressures ranging from about 1×10^{-6} to 2×10^{-4} Torr, for which the effects of collisions between atoms are negligible. The effect of resonance trapping was evident, and the resulting data were fit to the resonance trapping theories of Barrat and D'yakonov and Perel'. The resultant value of 19.3 ± 1.5 nanoseconds for the natural lifetime of the $^3P_1$ level does not agree with the calculated value of 10.2 ± 40% nanoseconds by Knox; some of the possible sources of this discrepency are discussed.

The situation in krypton is very similar to that in argon, except that the lithium fluoride window no longer gives the complete discrimination of the $^1P_1$ transition (1165 Å), because of the longer

wavelengths involved. However, the $^1P_1$ level lies 0.6 eV above the $^3P_1$ level, which means that the electron gun can be used to provide some further discrimination. An estimated 10% of the signal is due to the $^1P_1$ transition and, because its lifetime is almost the same as that of the $^3P_1$ transition, it is impossible to separate out its contribution to a given decay. The lifetime of the $^3P_1$ level was then investigated under conditions similar to those in argon. Later the excitation region was greatly reduced in size by placing the electron gun in a stainless steel cylinder 2.8 cm in diameter. The reduced effects of resonance trapping were noted, and the data were good enough to show that, of the existing theories of resonance trapping, the theory of D'yakonov and Perel' gives the best fit to these data. The several theories of resonance trapping are discussed, and it is shown that the theory of D'yakonov and Perel' agrees with the well-known theory due to Holstein, if one assumes a uniform spatial distribution of excited atoms. The measured value of 4.5 ± 0.6 nanoseconds for the lifetime of the $^3P_1$ level in krypton agrees well with the indirect measurements of Turner and Wilkinson, and it agrees well with the value calculated by Dow and Knox.

Measured Lifetimes for the First Excited J = 1 ($^3P_1$) Level in Argon and Krypton

by

John Ludwig Morack

A THESIS

submitted to

Oregon State University

in partial fulfillment of
the requirements for the
degree of

Doctor of Philosophy

June 1969

APPROVED:

Redacted for Privacy

Associate Professor of Physics

in charge of major

Redacted for Privacy

Chairman of Department of Physics

Redacted for Privacy

Dean of Graduate School

Date thesis is presented July 31, 1969

Typed by Clover Redfern for John Ludwig Morack

ACKNOWLEDGMENT

The author wishes to express his gratitude to Dr. Clifford Fairchild for proposing the research problem, for the many discussions concerning all aspects of the work, and for the conscientious help and encouragement needed to complete it.

TABLE OF CONTENTS

LIST OF FIGURES

MEASURED LIFETIMES FOR THE FIRST EXCITED J = 1 ($^3P_1$) LEVEL IN ARGON AND KRYPTON

INTRODUCTION

It is necessary to have a mathematical representation for an atomic system in order to understand and predict its properties. Even though the electromagnetic interactions involved in an atomic system are well known, only the simplest problem, that of an electron in the coulomb field of a spinless point positive charge, can be solved exactly. With the help of perturbation theory, it is possible to extend this problem to treat atomic hydrogen with a high degree of accuracy. However, it becomes necessary to resort to approximations in order to obtain wave functions for even the simplest of the multielectron atoms. The usual procedure is to try to obtain a solution of the Schrödinger equation in terms of single particle wave functions where magnetic interactions are neglected entirely and an average is taken over the residual coulomb interaction between electrons. Later, it is then possible to treat the neglected interactions using perturbation theory. A few years ago only the simplest of the multielectron atoms could be solved in this manner because of the difficulty of the calculations. With the advent of the modern computer this situation has changed somewhat, and it is now possible to obtain approximate solutions for complex atomic systems using this procedure. Thus,

the experimental determination of quantities such as energy levels, transition probabilities, magnetic moments, etc., which are characteristic of a particular atomic system, not only supplies fundamental information about the atom itself, but also provides the information necessary to evaluate the quality of the calculated wave functions for the atom.

The principal result of the experimental study to be described in this dissertation is the determination of the mean radiative lifetimes for some of the resonance electronic transitions (any transition to the ground state is a resonance transition) from the first excited multiplet in atomic argon and in krypton. Since it is the atomic transition probabilities rather than radiative lifetimes which appear as atomic constants, it is worthwhile to briefly review the relation between these quantitites. Consider a system of atoms in which $N(o)$ atoms have been excited at the time $t = 0$ to a state of energy E_ℓ. We would like to know the mean number $N(t)$ remaining in that state at the time t, assuming that the transition probabilities for spontaneous emission $S_{k\ell}$ are known for all k for which $E_k < E_\ell$ and that these transition probabilities are much larger than those for induced emission. The probability per second that one of the atoms in the state of energy E_ℓ will make a transition to any of the states of lower energy is given by

$$\lambda = \sum_k S_{k\ell} \,, \qquad 1.1$$

where the sum is over all levels $E_k < E_\ell$. In the time interval dt at t, the total number of such transitions will on the average be

$$N(t)\lambda\, dt \,, \qquad 1.2$$

since there are $N(t)$ atoms, all having λdt probability of undergoing a transition to a lower level. However, this quantity is just the decrease in $N(t)$ during the interval or

$$dN(t) = -N(t)\lambda\, dt \qquad 1.3$$

Integrating this from 0 to t, one gets

$$\int_0^t \frac{dN(t)}{N(t)} = -\lambda \int_0^t dt \quad \text{or} \quad \ln \frac{N(t)}{N(o)} = -\lambda t \qquad 1.4$$

Thus,

$$N(t) = N(o)e^{-\lambda t} \,. \qquad 1.5$$

That is, the number of atoms remaining in the initial state decreases exponentially from the original value $N(o)$ and, at a time $t = \frac{1}{\lambda}$, the number remaining is reduced by a factor of e^{-1}. The mean lifetime τ of this state is defined as the average time an atom spends in the state before making a transition. That is,

$$\tau = \frac{\int_0^\infty tN(t)dt}{\int_0^\infty N(t)dt} = \frac{N(o)}{N(o)} \frac{\int_0^\infty te^{-\lambda t}dt}{\int_0^\infty e^{-\lambda t}dt} = \frac{1}{\lambda} \qquad 1.6$$

or, using the definition of λ,

$$\tau = \left[\sum_k S_{k\ell} \right]^{-1} \qquad 1.7$$

If the ℓ^{th} level is a member of the first excited atomic multiplet, it can decay by an allowed transition only to the ground state. Furthermore, if the ground state multiplet contains only one level, as is the case for all the noble gases and many other atoms, then

$$\tau = \frac{1}{S_{o\ell}} \qquad 1.8$$

where the subscript o denotes the single level of the ground state multiplet. Thus, the mean radiative lifetime equals the inverse of the transition probability for the special case of an allowed transition from the first excited multiplet to a single ground state.

For any atom the resonance transition energies are large compared to the energy differences between excited states; consequently, in the calculation of dipole matrix elements, the radial integral will be typically considerably smaller for a resonance transition than for an intermediate transition. Because of this, the measurement of the

transition probability for a resonance transition is usually a more sensitive test of the quality of calculated radial wave functions than is the same measurement for an intermediate transition.

In order to understand the equilibrium properties (e. g. , temperature, energy distribution, degree of ionization, etc.) of gas plasmas, it is necessary to know quantities such as collision cross sections for excitation and transition probabilities. As an example of such a plasma, consider a star, the light from which constitutes nearly all the information about the star that we have. Yet, from an analysis of these signals, we are able to determine, among other things, its atomic constituents and its motion relative to the earth. With a knowledge of all the relevant atomic properties, it may also be possible to give a useful representation of stellar atmospheres.

Experimental Difficulties

There are two undesirable environmental effects which are present in any lifetime measurement. These are due to changes in the concentration of atoms in the excited level under study by cascade transitions from higher lying levels and by the collisional exchange of excitation energy. Either of these effects make it necessary to add a term or terms to the differential equation for the concentration of excited states (Equation 1. 3) and, therefore, destroys the simple relationship between the mean lifetime and the transition probability for

the state. For this reason, it is usually advantageous to minimize these effects.

There are other difficulties which occur and cannot be avoided experimentally. Because of the large energy separation of the first excited multiplet from the ground state in atomic systems, the wavelengths of many atomic resonance transitions are in the extreme ultraviolet, that is, in the wavelength region below about 1500 Å. The wavelengths for all of the resonance transitions in the noble gases are in this spectral region. Because all optical materials are nearly opaque in this region of the spectrum, methods of determining lifetimes which require high resolution spectrographs or polarized light sources are difficult.

Another problem that is peculiar only to lifetime measurements for resonance transitions is resonance trapping. In simplified terms, this process can be described in the following way. An atom in an excited state decays by emitting a photon which, on the average, has just the proper frequency to excite a neighboring atom to the same excited state. This process may be repeated many times before the photon is actually observed, and the photon is said to have been "resonantly trapped." That is, the period of time that elapses before the photon is observed is too long and will be a function of the pressure of the gas. This process is a contributing factor only in the case of resonance transitions. In the case of intermediate transitions, the

concentration of excited state atoms, i. e., those capable of absorbing a photon, is so small that the chance that a given photon will be absorbed even once is negligible.

In reality, resonance trapping is a more complex problem than is implied by the simplified description given above. The frequency dependence of the absorption and emission lines involved make the problem difficult to treat theoretically. Several successful attempts have been made to analyze resonance trapping, but they all contain many approximations. Any lifetime measurement for a resonance transition will involve the effects due to resonance trapping and, therefore, test these approximations.

Methods of Measuring Atomic Lifetimes

The several methods that have been devised to measure atomic lifetimes can be classified as either direct or indirect. The direct method is simply a determination of the number of atoms in an excited state as a function of time in the absence of any excitation processes. There is, of course, no way to tell if an atom is in an excited state; however, as an atom decays, a photon is emitted. Since the number of photons emitted in a time dt is proportional to the number of excited atoms existing at the time t, a knowledge of the resulting light intensity as a function of time is equivalent to knowing the number of atoms in an excited state as a function of time.

Most of the experiments performed fall into the class of indirect measurements made on intermediate transitions in the visible wavelength region (33, p. 145-151; 17, p. 1-42). Because of the difficulties described in the previous section, it is only recently that these and other new methods have been used to measure mean lifetimes for resonance transitions.

Let us briefly discuss some of the methods that have been successful for the case of extreme ultraviolet resonance transitions (1, 7, 30, 31, 37, 38, 41, 42). The zero-field level crossing method or Hanle effect has been used recently to measure the lifetimes of the $(5p^5 6s)$ $^3P_1$ and $^1P_1$ levels in xenon (1). Level crossings are observed experimentally by noting a change in the angular distribution or the polarization of radiation from atoms excited by resonance absorption as a function of the magnitude of an applied magnetic field. These effects can be described by a classical theory of damped oscillating dipoles precessing with their Larmor frequency (33, p. 264-267), or by the quantum mechanical theory of interference effects in resonance fluorescence (8). The resonance transition wavelengths for the first excited $^1P_1$ and $^3P_1$ levels in xenon are 1296 Å and 1470 Å, respectively. Methods involving the use of polarized light and atomic excitation by resonance fluorescence are very difficult in this wavelength region. Additionally, the measured lifetimes must be extrapolated to zero pressure because of resonance trapping. The Hanle effect does have

the advantage of being able to measure other quantities, such as the g values of the levels involved.

Another method that has been used successfully in the extreme ultraviolet is that of resonance absorption (37, 38, 42). This method consists of determining the frequency dependent linear absorption coefficient for a gas by observing the transmission coefficient I/I_o as a function of distance through the gas. For a beam of parallel light consisting of a single emission line, the intensity of light transmitted through the cell for a distance x is given by

$$I = \int_{-\infty}^{\infty} I_o(\nu) \exp [-k(\nu)x] d\nu \qquad 1.9$$

The lifetime is directly related to $k(\nu)$, so the problem reduces to finding $k(\nu)$. This is a very difficult problem because it is necessary to determine the incident intensity per unit frequency interval $I_o(\nu)$ which involves not only the natural line width of the emission line, but its doppler broadening, collisional broadening, and self reversal in the light source. Likewise, the same problems of line broadening occur in the absorption so that, in practice, the actual fit to the data requires several parameters and, therefore, a wide variety of different experimental conditions in order to get the desired precision for the lifetime.

A method utilizing saturated resonance trapping has been used

by R. Turner (41) to measure lifetimes for the $(4p^5 5s)\ ^3P_1$ level in krypton, and is, therefore, of special interest here. He examined the decaying light signal from a pulsed discharge in krypton gas in the pressure region from 0. 2 to 6. 0 Torr. At this pressure it was found necessary to include the effects due to collisions between excited state atoms and ground state atoms and the effects of resonance trapping. Using the theoretical work of Holstein (25, 26), it was estimated that in this pressure region the lifetime of the trapped resonance radiation is determined by pressure broadening of the resonance line. Under these conditions, Holstein has shown that the decay constant is independent of gas pressure. A two component decay was observed for these experimental conditions. One component, a pressure dependent slow decay having a lifetime on the order of 100 microseconds, was explained in terms of diffusion of metastable atoms to the walls of the chamber and collisional processes involving excited atoms and ground state atoms. The fast decay, having a lifetime of about the ten microseconds, was found to be pressure independent and, therefore, due entirely to resonance trapping of the pressure broadened line. The experiment was done for several geometries, and, from the fast decay, a value of 4.15×10^{-9} seconds was determined for the natural lifetime of the $(4p^5 5s)\ ^3P_1$ level of krypton. Under these experimental conditions the processes involved are actually much more complicated than the simple model that Turner has taken for the system.

For instance, one would not be surprised to find that cascading from higher levels to the first excited multiplet would modify the decay. Because of the complexity of the atomic system, it was decided that a direct measurement of the lifetime for this level was warranted as a check on the approximations made by Turner.

Because of the definition of the mean lifetime for an atomic state, the direct method is the most straightforward and least ambiguous of the methods. The recently developed beam foil method (7) has been quite successful for extreme ultraviolet transitions. Ions from a Van de Graaff accelerator are passed through a thin foil where the beam atoms are excited to all levels of excitation and ionization. The radiative decay of a particular level is determined by measuring the intensity in an appropriate emission line from a small portion of the beam as a function of the downstream distance between the excitation foil and the viewing aperture. The principal disadvantage of this method is that cascading from upper levels cannot be avoided. However, using this method, one is able to investigate lifetimes of transitions occurring in virtually any stage of ionization; thus, it is the only method capable of examining many transitions of astronomical interest.

The method chosen for the present investigation (36) is a modified delayed coincidence method similar to those which have been used previously to measure decay rates for optical transitions outside the

ultraviolet (5, 6, 23, 27, 28). The method is illustrated in Figure 1. The atomic excitation is produced by bombarding a gas sample with a pulsed beam of electrons. For a given pulse of electrons the light output from the gas will increase until the excitation is terminated, and then, under ideal conditions, it will decrease as a single exponential decay. Typically, this decaying light signal when detected and amplified will be too weak to be displayed directly or with a sampling oscilloscope. Instead, at some delay time t after the excitation is terminated, the light detector itself is gated to sample the light output for a time interval Δt. Then, using a high gain dc amplifier, the dc level of the detector output is averaged over many decays. As will be shown later, for an exponentially decaying light signal, the detector output is proportional to the light intensity at the beginning of the sampling interval. Thus the decay curve is reconstructed by varying the delay time t in discrete steps.

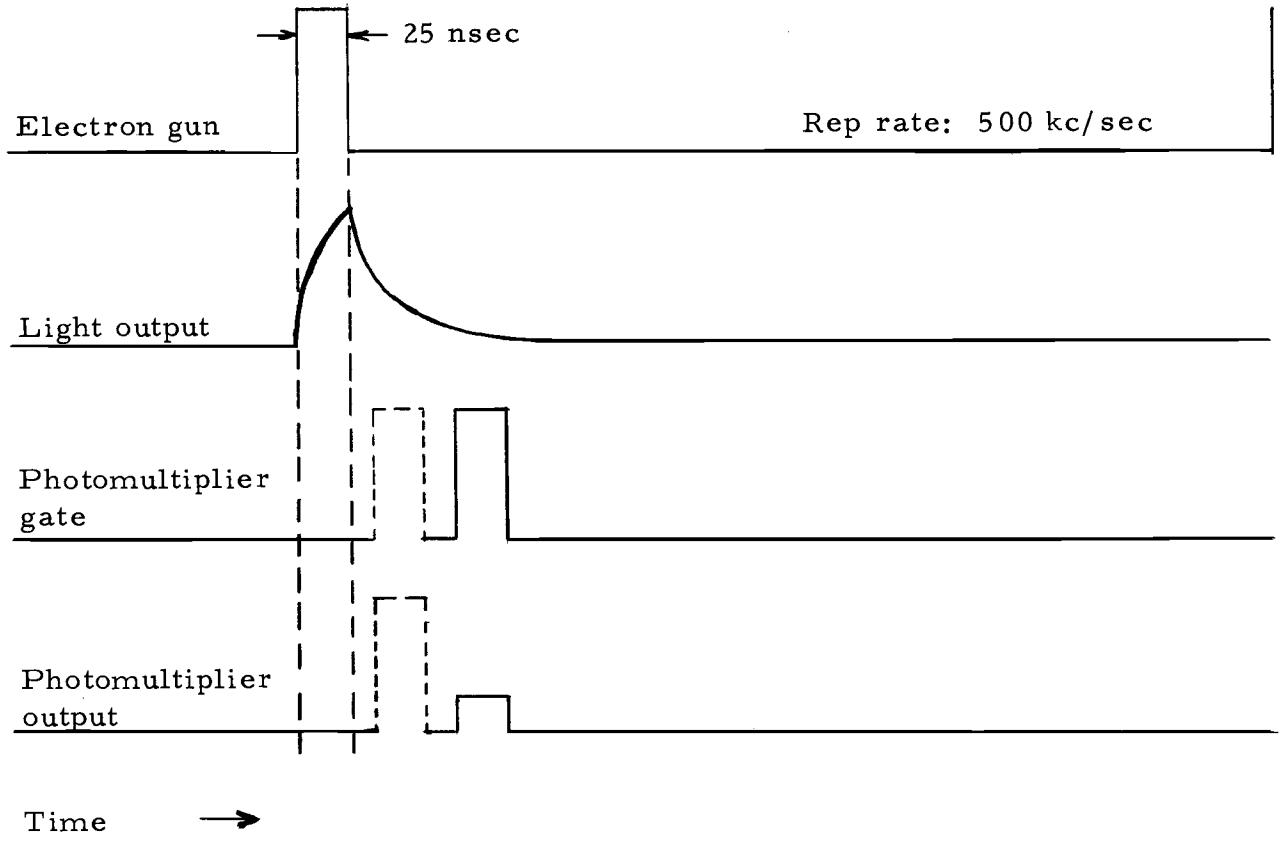

Figure 1. Sequence of events in modified delayed-coincidence method. The numbers shown are typical values used in the argon experiment.

EXPERIMENTAL SETUP

The apparatus described in this chapter was designed to be capable of measuring lifetimes for extreme ultraviolet resonance transitions, lifetimes which might be as short as a few nanoseconds. Furthermore, the gases under study had to be of low enough pressures so that the effects of collisional processes would be negligible. Also, in order to eliminate the effects of cascading, the excitation energy supplied to the gas had to be controllable to the extent that any atom would be selectively excited to its first excited multiplet. In order to satisfy these requirements, electron bombardment is the only practical mechanism for excitation of the gas sample, although this type of experiment has been done in the visible wavelength region using light pulses transmitted by a pulsed Kerr cell (27). However, the construction of such a cell for extreme ultraviolet wavelengths is not feasible at present.

The assembled apparatus is shown schematically in Figure 2; the details of the detector, the electron gun, and the excitation region will be discussed in detail later.

Excitation Chamber Vacuum System

It is necessary to employ a vacuum system capable of attaining pressures below 10^{-4} Torr in order to eliminate collisional effects.

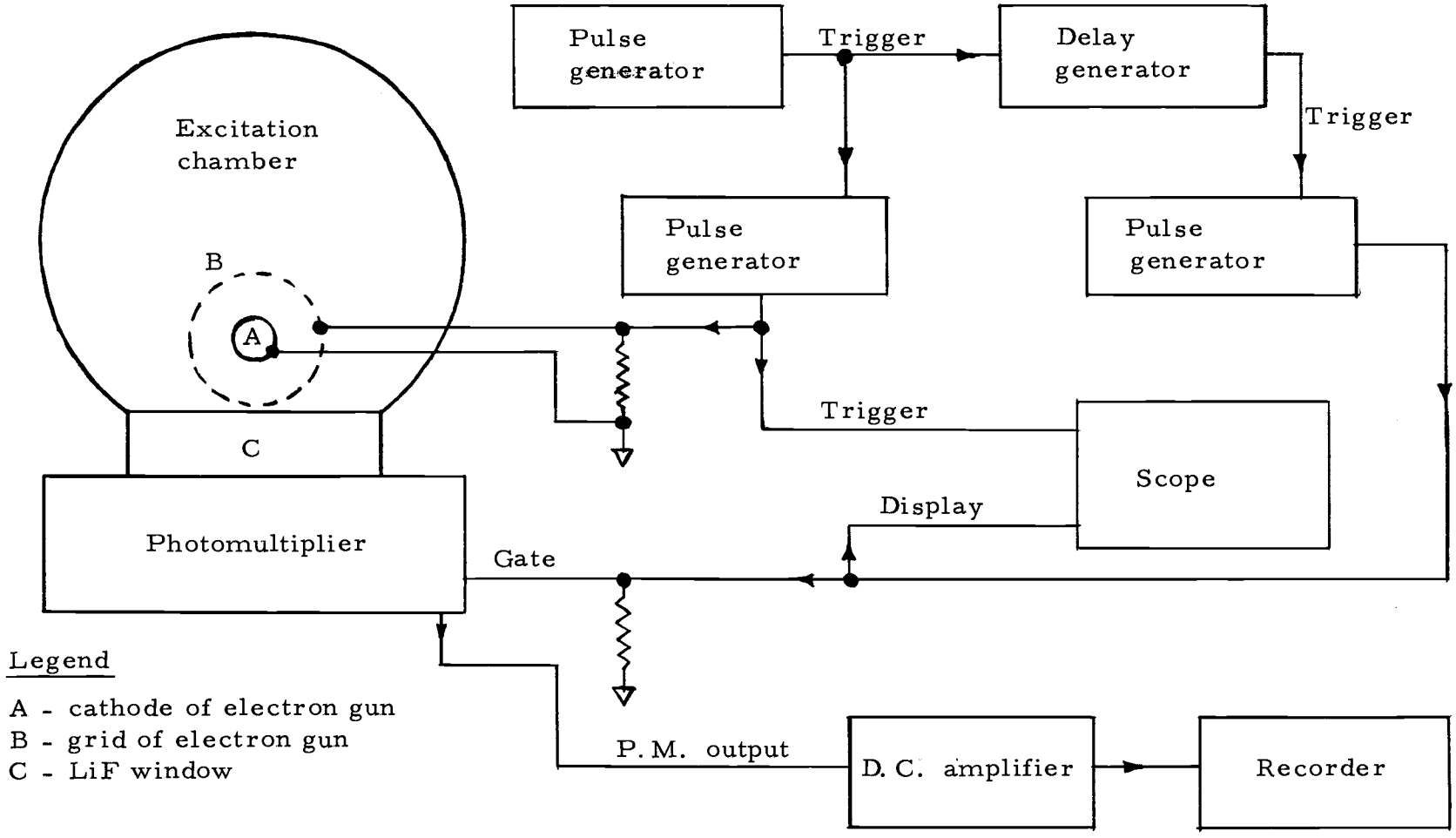

Figure 2. Schematic diagram of the apparatus.

(At 2.0×10^{-4} Torr the average gas kinetic collision frequency is about 10^{3} sec^{-1}.) Furthermore, to minimize the effects of background gases, it was decided to pump to a base pressure much lower than this and then let the gas sample flow continuously through the excitation chamber.

The four liter excitation chamber is a stainless steel cylinder with a radius of seven centimeters and with a lithium fluoride window set in about three centimeters, as indicated in Figure 2. The excitation chamber is pumped to a base pressure of about 10^{-7} Torr with a two inch diffusion pump and a pellet type trap filled with Sorbent A (Trademark Consolidated Vacuum Corporation). The Sorbent A is baked under vacuum to drive off absorbed water vapor and serves as an oil getter between the pumping system and the excitation chamber. Therefore, the Sorbent A is changed at each opening of the vacuum system to inhibit contamination of the excitation chamber and electron gun by pump oils during the following bakeout. A liquid nitrogen trap is placed between the forepump and the diffusion pump, and the combined effect of it and the pellet trap is to reduce the base pressure from about 10^{-6} to 10^{-7} Torr.

At present, the base pressure of the system is probably limited by small leaks through the stem of the pneumatic gate valve located between the diffusion pump and the excitation chamber. This valve is set to close during an electrical power failure to prevent damage of

the excitation chamber by pump oils. Furthermore, it is closed during the initial starting period of the diffusion pump to prevent back streaming of diffusion pump oil into the excitation chamber. For these reasons, the gate valve has been retained in the system.

Gas Handling and Pressure Measurement

A steady flow of the gas sample to be studied is established with a standard gas handling system. Research grade gas is let in through a Matheson Model 18 ultrapure pressure regulator (with an advertised inboard leak rate less than 8×10^{-10} cc/sec) followed by a fine control needle valve. Pressure control in the excitation region is maintained to ± 5% over long periods of time in the pressure region from 10^{-6} to 10^{-4} Torr.

The gas pressures are measured with an ionization gauge and then corrected for differences in ionization probability of the gases. In the experiment on argon the pressure gauge supply was a Bon-De Model BD-20C; this gauge and supply were supplemented during the krypton experiment by a Varian dual range ionization gauge supply Model 971-0014, a low range nude gauge (pressure range 10^{-4} to 10^{-11} Torr), and a high range nude gauge (pressure range 10^{-1} to 1 Torr). Since both of the Varian gauges are mounted inside the excitation chamber, they must be turned off during the actual lifetime measurements because it has not been possible to completely shield the

detector from radiation produced by their electron bombardment of the gas. Consequently, after the pressure is determined, it is monitored during the lifetime measurements by the Bon-De gauge which is mounted on an appendage to the system.

Electron Gun Electronics

The electronics in the system had to be able to provide pulses of a few nanoseconds duration with rise and fall times of the order of one nanosecond. Also, the delay time between the photomultiplier pulse and the electron gun pulse had to be measured to within a few tenths of a nanosecond.

As shown in Figure 2, an E-H Model 120B pulse generator is used as a clock for the system. Its output, capable of repetition rates up to ten MHz, is used to trigger the electron gun pulse generator and the delay generator in the photomultiplier pulsing circuit.

The electron gun pulse generator is an E-H Model 120D which has a variable output pulse from 0 to 20 volts and variable pulse widths from a few to 100 nanoseconds. These pulses are nearly rectangular with rise and fall times which are typically one nanosecond. The wave form of a typical electron gun pulse used during the krypton experiment is shown in Figure 3.

Electron Gun

A 6SJ7 tube was chosen as an electron gun because, being a high frequency tube, the control grid and cathode are very close to each other, thus allowing the electron beam to be terminated very quickly. Also, the cylindrical geometry of the tube is just that called for by the several theories of resonance trapping.

For the argon experiment a glass 6SJ7 was used. The plastic tube socket was removed, the glass cut around the tube base, and then the top part of the glass tube was removed. The plate and all the grids except the control grid were removed. Thus, the electron gun consisted of the control grid and the indirectly heated cathode parts of the tube as shown in Figure 5. The electron gun was placed in the vacuum system as soon as possible, which was then pumped to about 10^{-6} Torr with the electron gun filament at 1.5 volts. Then the gun was activated by slowly increasing the filament voltage to 9.5 volts, at which time the cathode material would be almost completely outgassed.

In order to achieve the best possible termination for the electron gun pulser and to prevent ringing of the pulse at the electron gun, a 50 ohm termination was placed across the electron gun lead-in wires just outside the vacuum system. The cathode was grounded and the control grid pulsed positive to turn on the electron gun. Actually,

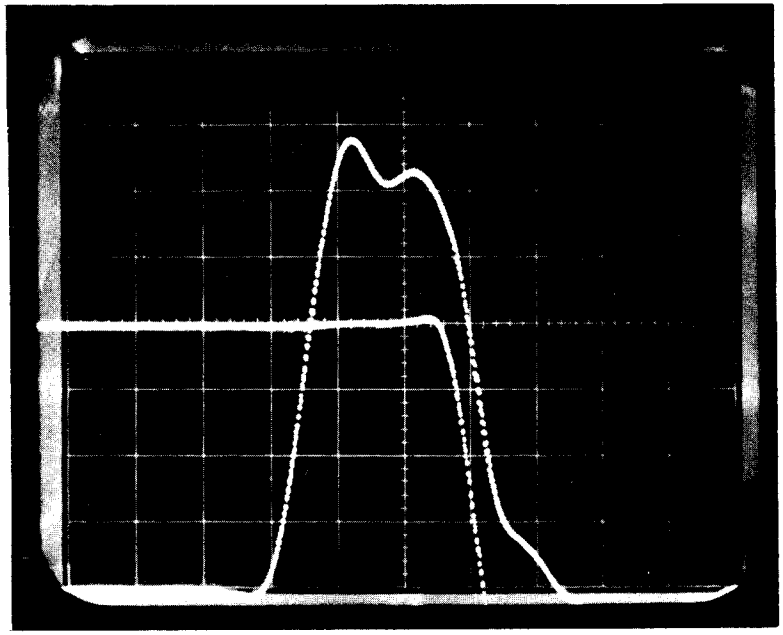

Vertical Deflection (2 volts/div)

Time (2 nsec/div)

Figure 3. Waveform for the electron gun pulse (positive) used for the Krypton experiment. Also shown is the leading edge of the photomultiplier gate pulse (negative deflection). For this display the turnoff of the electron gun pulse has been delayed 20.0 nsec with respect to the leading edge of the gate pulse.

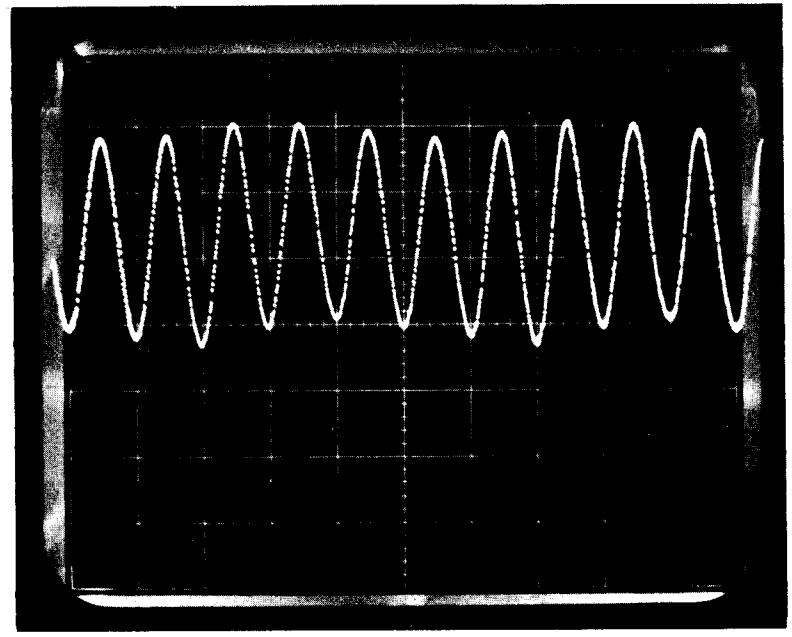

Time (2 nsec/div)

Figure 4. Calibration waveform (2 nsec/cycle) from a Tektronix Model 184 Time Mark Generator displayed on a Tektronix Model 561 Sampling Oscilloscope.

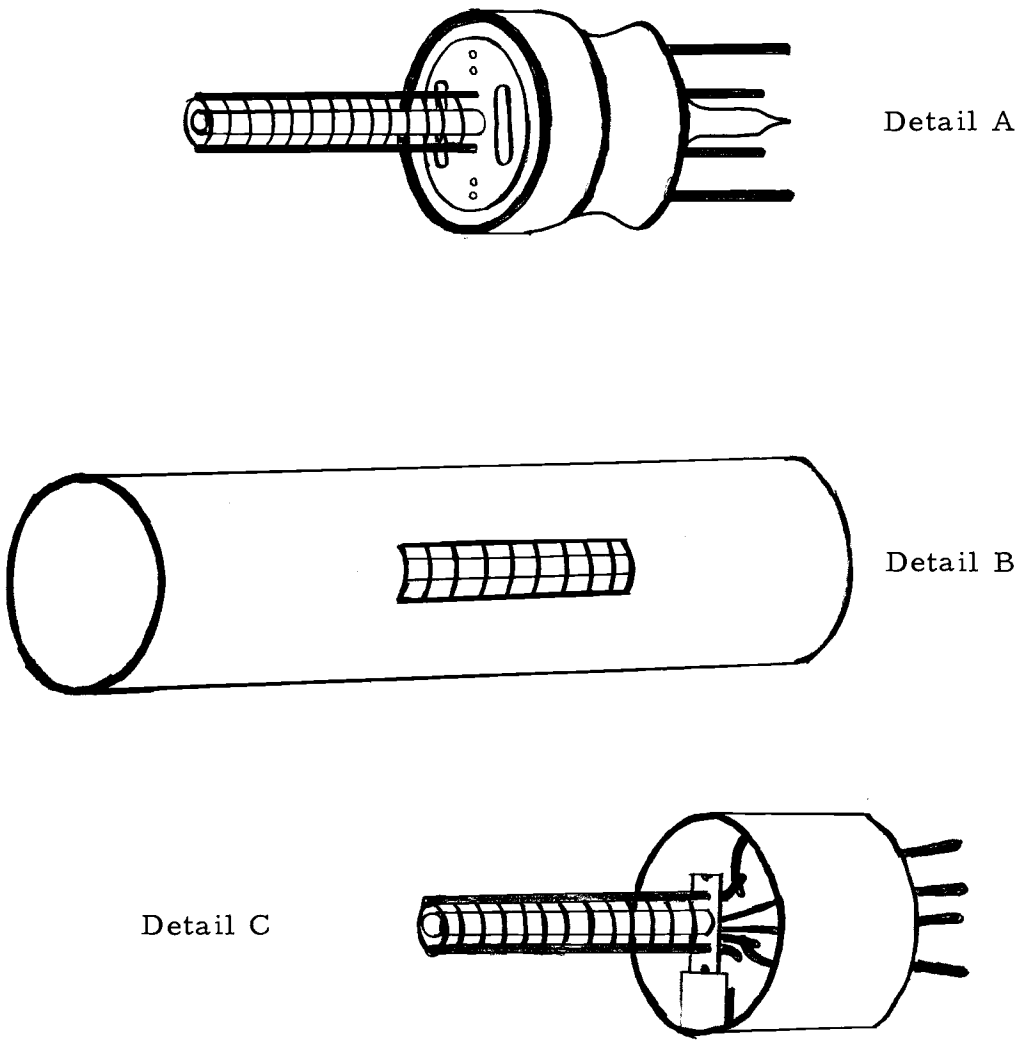

Figure 5. Electron gun used in argon experiment (Detail A). Excitation enclosure (Detail B) and electron gun (Detail C) used in the krypton experiment.

several different pulsing configurations were tried, but this one proved to have the shortest turn-off time. The total turn-off time for the electron excitation is determined by the fall time of the applied pulse and the effects of electron transit times in the excitation region. For this configuration, the turn-off time was determined from the early stages of the light output decay curve to be at the most a few nanoseconds.

The electron gun is operated space charge limited with the filament overdriven at 9.5 volts instead of the recommended 6.5 volts in order to increase the emission. It is conjectured that the atomic excitation occurs in a small region near the control grid because this should be the only region where the electrons have enough energy to excite the gas.

The filament voltage was supplied by a Variac and a filament transformer. In the later experiment on krypton this ac supply was replaced by a regulated negative dc supply in order to reduce the effect of atomic excitation, presumed to be due to the electric field produced by the filament.

In order to investigate fully the effects of resonance trapping, data were taken with the center of the electron gun at several different positions near the lithium fluoride window and with the axis of the gun either vertical or horizontal. In the later experiment on krypton the control grid and cathode structure of the 6SJ7 were completely

removed from the tube base and spot welded into a specially made holder which then could be slipped into a stainless steel cylinder having a diameter of 2.8 centimeters. This cylinder has a small opening cut in it in order for the photomultiplier to view the decaying light signal. The entire assembly is shown in Figure 5.

Photomultiplier Electronics

Again referring to Figure 2, the delay generator, an E-H Model 921 which can produce continuously variable time delays from fifty to several hundred nanoseconds, is used to trigger a second E-H Model 120D pulse generator which, in turn, is used to gate the photomultiplier. The gate pulse is simultaneously displayed on a Tektronix 519 oscilloscope, which is triggered by the electron gun pulse, to determine the time relationship between the shutoff of the excitation and the gating of the photomultiplier. The calibration of the time sweep of the Model 519 oscilloscope was checked before and after the argon experiment at the Tektronix plant in Beaverton, Oregon. To within the accuracy of approximately 1% of these checks, no systematic drifts were detectable.

In the experiment on krypton the Model 519 oscilloscope was replaced by a Type 3S1 dual trace sampling plug-in unit in conjunction with a Type 3T77A sampling sweep plug-in unit on a Tektronix 561A oscilloscope. The rise time of the sampling unit is 0.35

nanosecond whereas the Model 519 has a rise time of 0. 23 nanosecond, but the added maximum sensitivity (2 millivolts/cm compared to 9. 5 volts/cm), the faster sweep rate (a maximum of 0. 1 nsec/cm), and the dual input of the sampling oscilloscope makes it the more useful oscilloscope for this application. A calibration of the time sweep on the sampling oscilloscope, made in our laboratory with a Tektronix Time-Mark Generator Type 184, is shown in Figure 4. The Time-Mark Generator is a crystal controlled oscillator adjusted at the factory to a 10 MHz primary standard.

Light Detection System

The last part of the apparatus to be described is the light detection system. A Bendix Model M308 high resistance strip magnetic electron multiplier, hereafter referred to as an MEM, was chosen as a photomultiplier for the following reasons. The MEM has a tungsten plate for a cathode whose quantum efficiency as a function of wavelength is shown in Figure 6. As can be seen, it has essentially no response above 1500 Å because of the high work function of the cathode. This property makes it ideal as an extreme ultraviolet detector. It is also well suited for very weak signals because the cathode gives rise to practically no dark current (none detected with an ammeter sensitivity of 10^{-13} amperes). Additionally, the MEM has no activated surfaces and thus can be removed from the vacuum system without

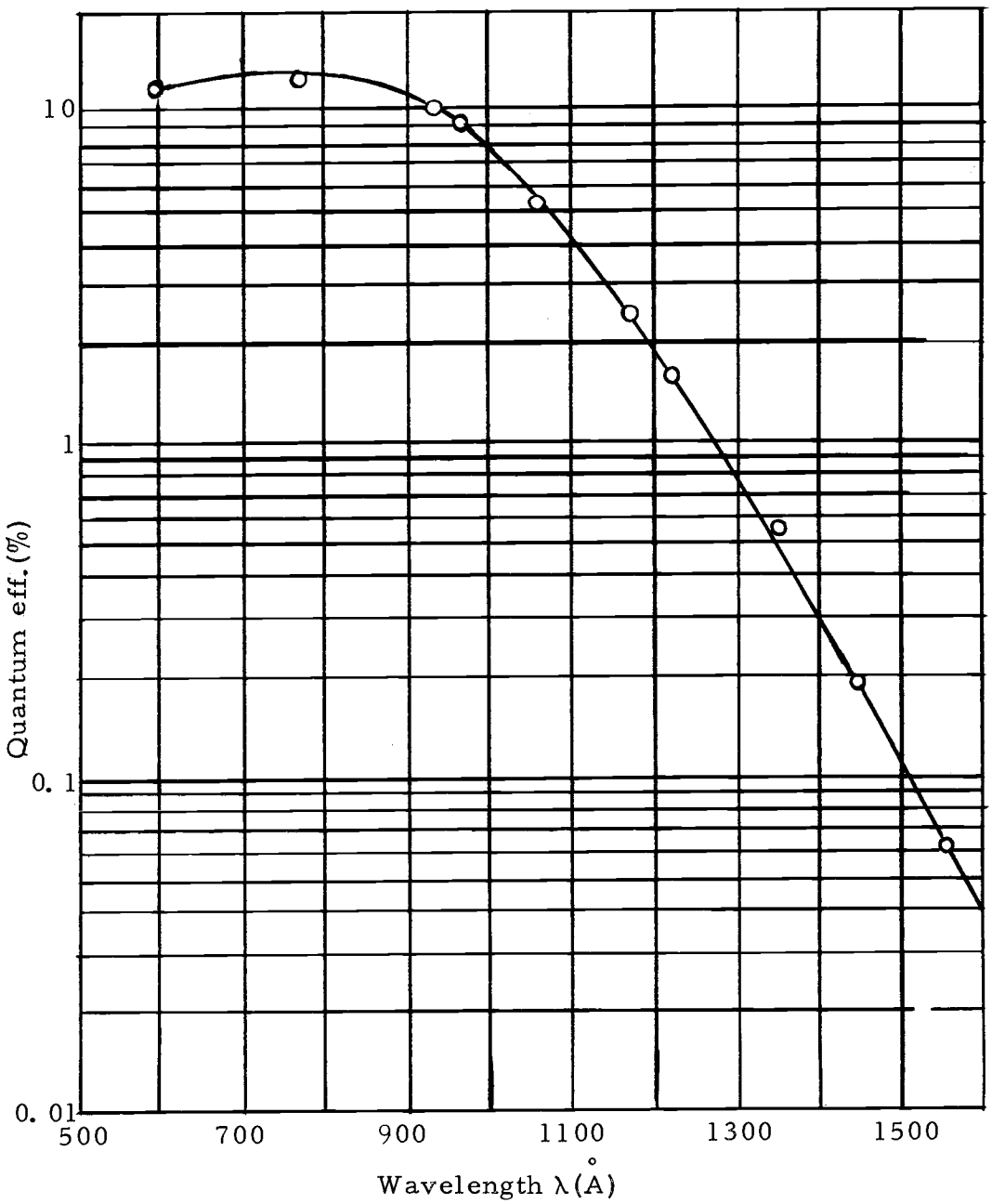

Figure 6. Quantum efficiency of the Bendix Model M308 magnetic electron multiplier. (Reprinted from the M308 Instruction Manual.)

damage to the cathode and dynode structure. However, the modified delayed coincidence method requires that the light detector be gated on for a period of a few nanoseconds in order to sample the decaying light from the excitation chamber. In order to accomplish this, the anode section of the MEM was modified to a dual anode configuration.

To facilitate the description of this modification, it is necessary to briefly describe the operation of the MEM (18, 24). A cross sectional view of the modified MEM is given schematically in Figure 7. The MEM is comprised of a 90% optically transparent metallic entrance grid, a tungsten cathode, a coated glass dynode strip, a coated glass field strip, and an anode. The dynode and field strips are coated with a high resistance material, and each measures about 100 megohms along its 4.5 cm length. They are mounted parallel to each other with a separation of 0.25 cm inside a small permanent magnetic structure which produces a uniform magnetic field of about 400 gauss perpendicular to the plane of Figure 7. In Figure 7 the thin solid lines indicate conductors and the numbers give nominal voltages applied to the MEM. In the unmodified MEM a stainless steel anode was placed between FS01 and DS01.

Electrons ejected with essentially zero velocity from the cathode by a photon find themselves in a crossed electric and magnetic field. The path for each electron is a cycloid whose cusps fall along an equipotential line as shown in Figure 7. The parametric equations for a

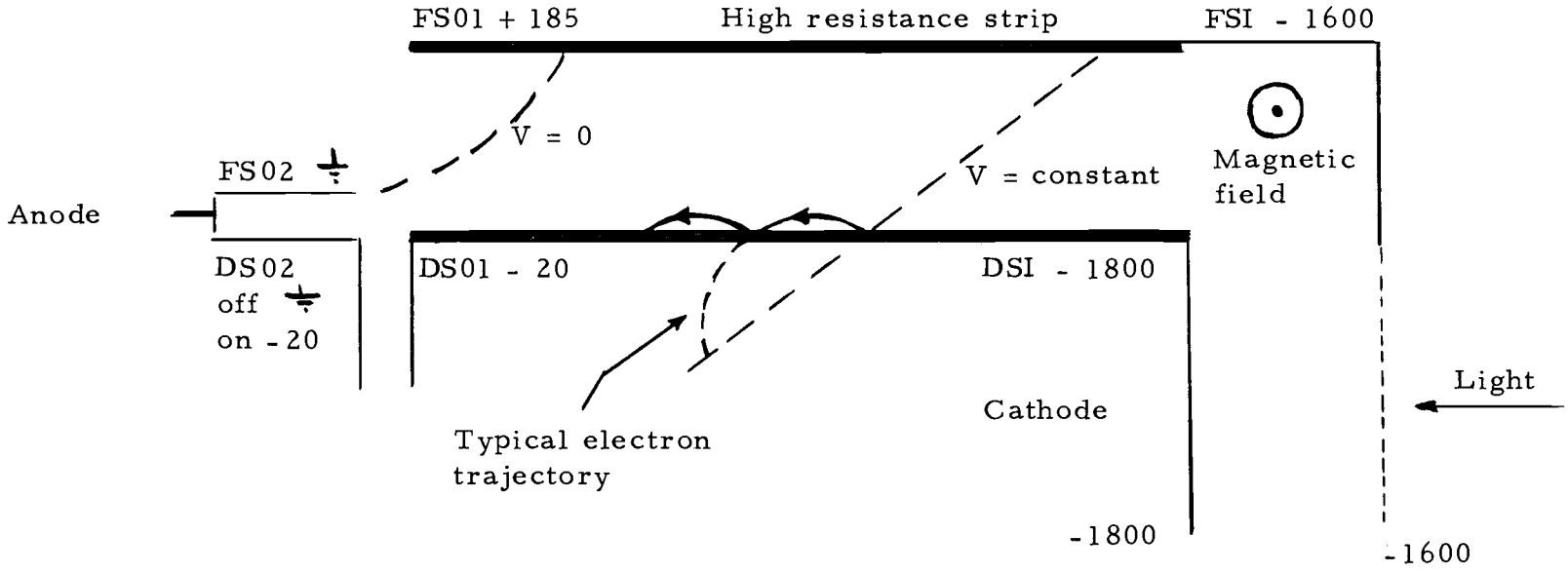

Figure 7. Schematic diagram of the modified magnetic electron multiplier.

cycloid are

$$x = a(\phi - \sin\phi)$$
$$y = a(1-\cos\phi)\ , \qquad 2.1$$

where

$$a = \frac{m}{e}\frac{E}{B^2}\ , \qquad 2.2$$

and

$$\phi = \omega t = \frac{eBt}{m}\ . \qquad 2.3$$

Here m and e are respectively the mass and charge of an electron, E is the electric field strength and B is the magnetic field. The angle that the cycloid is tipped, that is, the angle that the equipotential plane makes with the dynode strip is given by

$$\tan\beta = \frac{E_{\parallel}}{E_{\perp}} = \frac{y_s}{x_s} = \frac{1-\cos\phi_s}{\phi_s - \sin\phi_s} \qquad 2.4$$

where $E_{\parallel}$ is the component of electric field strength along the dynode strip, $E_{\perp}$ is the component of electric field perpendicular to the dynode strip, and the subscript s denotes the values of the quantities at a distance s along the dynode strip, where the cycloid intercepts the dynode strip, that is, the point where the electrons collide with the dynode strip. Solving this equation graphically, the value of ϕ_s for this particular configuration is $\phi_s = 3.51$ radians. Thus, it is a simple matter to calculate s, the distance per stage

of electron multiplication, since

$$s = \frac{x_s}{\cos\beta} = \frac{m}{eB^2}\frac{E}{\cos\beta}(\phi_s - \sin\phi_s) = 0.138 \text{ cm} . \qquad 2.5$$

Therefore, the total number of stages is

$$\text{Number of stages} = \frac{\text{length of dynode strip available for multiplication}}{s}$$

$$= \frac{4.35 \text{ cm}}{0.138 \text{ cm}} = 31.6 \text{ stages} . \qquad 2.6$$

Likewise, the time per stage is

$$t_s = \frac{\phi_s}{\omega} = \frac{m\phi_s}{eB} = 0.50 \times 10^{-9} \text{ sec} . \qquad 2.7$$

In these calculations the effects of space charge and the variable initial momenta of the photoelectrons and the secondary electrons have been neglected. These effects, which give rise to the production (by each photoelectron) of an anode current pulse of finite width, will appear later in the analysis of the sampling technique. Assuming that the center of such a pulse corresponds to electrons ejected with no initial momenta, the time required for this pulse to traverse the entire length of the dynode strip is given by

$$\bar{t} = \text{number of stages} \times t_s = 15.8 \times 10^{-9} \text{ sec} . \qquad 2.8$$

A similar analysis shows that in the cathode region, where there is no multiplication, it takes an electron 3.33×10^{-9} seconds to move the full length of the cathode.

It is also of interest to calculate the distance between an equipotential plane and the apex of the path labelled "typical electron trajectory" in Figure 7. This is

$$y_{max} = \frac{m}{e} \frac{E}{B^2} (1-\cos \pi) = 0.64 \text{ mm.} \qquad 2.9$$

It is the smallness of this quantity that suggested modifying the anode section of the multiplier. With the voltage pulses available using an E-H Model 120D pulser, it is possible to maintain the proper electric field strength between two small, closely spaced conducting plates and channel the electrons to and away from the anode, as shown in Figure 7. The anode current of the multiplier is sampled by pulsing the DS02 plate. With this plate at ground potential, the electrons are deflected into the channel between the DS02 and DS01 plates and thus are not collected. With the DS02 plate potential at -20 volts, these electrons are deflected into the channel between the DS02 and FS02 plates, and then accelerated to the anode. The actual separation between the sets of plates was chosen to be 0.65 mm (0.025"). For a nominal pulse voltage of 25 volts, $y_{max} = 0.28$ mm or about half that of the plate separations. That is, the values chosen for the anode structure plate separations represent a compromise between the requirement for a low voltage sampling pulse and allowances for

fringing of the applied electric and magnetic fields. It is noteworthy that with the plates biased in the off configuration, no signal at the anode is detected. The length represented by the FS02 line in Figure 7 was also kept small (less than 4 mm) in order that the magnetic field for the modified anode section could be supplied by the standard MEM magnet structure. Because of the very small size of the anode structure, the stray capacitance of the DS02 plate is kept very small, which means that the actual switching of the electrons occurs in a time about equal to the rise time of the applied pulse.

In order to insure that the decay measured is the same as that of the incident light signal, it is necessary to investigate in some detail the effects of the finite length of the cathode, the spreading and the shape of the electron pulses during multiplication, and the finite sampling time. To do this, let the cathode be uniformly illuminated with light from a source which decays exponentially according to the relationship

$$I = I_o e^{-\lambda t_o} . \qquad 2.10$$

In Figure 8 the cathode is denoted by the line segment 0 to y_c. The photoelectron current at the point o (where multiplication of the signal begins) from an infinitesimal length dy of the cathode at y is

$$di_p(t_o) = -\frac{QI_o}{y_c} e^{-\lambda(t_o - y/v_y)} dy , \qquad 2.11$$

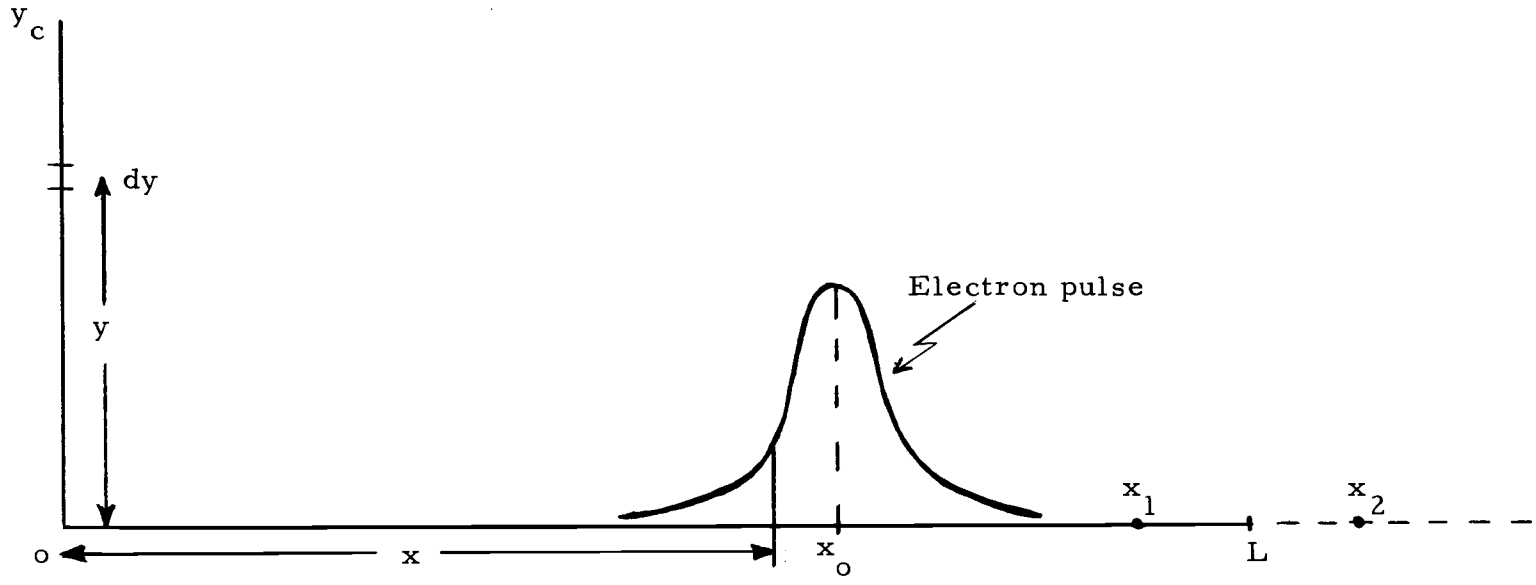

Figure 8. Coordinates used in the discussion of electron multiplication in the magnetic electron multiplier.

where Q is the average photoelectron current per unit of incident intensity, and v_y is the average velocity of photoelectrons along the cathode (assumed here to be the same for all the electrons). We note that for an elapsed time, $t_o < y_c/v_y = t_c$, only part of the cathode ($y_{max} = v_y t_o$) contributes to the total current at 0. This total current, then, is

$$i_p(t_o < t_c) = -\frac{QI_o}{y_c} e^{-\lambda t_o} \int_0^{y_{max}} e^{\lambda y/v_y} dy = -\frac{QI_o v_y}{y_c \lambda} (1 - e^{-\lambda t_o}). \qquad 2.12$$

That is, before a contribution is received from the entire cathode, the signal at the point o is actually increasing! For the case $t_o \geq \frac{y_c}{v_y} = t_c = 3.33 \times 10^{-9}$ sec (as calculated earlier),

$$i_p(t_o \geq t_c) = -\frac{QI_o v_y}{\lambda y_c} e^{-\lambda t_o} [e^{\lambda y_c/v_y} - 1]. \qquad 2.13$$

Only after a time t_c does the signal at the beginning of the multiplication section of the MEM show the characteristic decay of the incident light.

In this derivation for the photoelectron current, i_p, at the point o, it was assumed that all the photoelectrons moved with the same average velocity v_y. This is only true for the condition that all the photoelectrons are ejected from the cathode with negligible

momenta. . In reality there will be a spread in their initial momenta which will result in a slightly different average velocity for each electron. For the applications to be discussed here, the energy of the incident photons will be only slightly greater than the work function of the cathode, thus, the spread in initial momenta will be small. Additionally, since the electrons make no collisions with the cathode and the distance of travel along the cathode is small, the effect of the spread in v_y will be very small compared to the spread in average velocity which is accrued along the dynode strip; therefore, although it is not necessary, it will be convenient to neglect the spread in v_y.

The effect of the spread in the initial momenta of secondary electrons produced in the multiplier section of the MEM cannot be neglected, because here the lines of equal potential are tipped (Refer to Figure 7) so that electrons will collide with the dynode strip with an energy of about 60 eV. That is, each colliding electron gives rise to the ejection of an average of about 1. 5 electrons from the dynode strip, with a spread in initial momenta which cannot be neglected. As this pulse of electrons moves down the dynode strip, the effect of this spread in momenta will be compounded at each collision with the dynode strip. Therefore, the pulse of electrons due to a single photoelectron will not only increase in amplitude as it moves down the dynode strip, but will have a finite width associated with it which will be increasing along the dynode strip.

In determining the relationship between the time t_o described previously and the measured sampling time at the anode, it is convenient to represent the electron pulse for each photoelectron by a function $f(x-x_o)$ which gives the amplitude of the electron pulse centered at x_o as a function of x along the dynode strip. Such a pulse is shown in Figure 8, where the dynode strip is represented by the line segment o to L. Since, at the anode, each of these pulses contains about 10^6 electrons, it will be assumed that they are all identical. Now

$$x_o = v_x(t-t_o) , \qquad 2.14$$

where v_x is the average velocity of the electron pulse down the dynode strip and t is the time. The beginning of the anode section is located at $x = L$, so the function $f(x-x_o)$ must be evaluated at $x = L$, where the current is

$$i_a(t) = \int_0^t f(L-v_x(t-t_o))i_p(t_o)dt_o . \qquad 2.15$$

As a simple example, consider the case where $f(x-x_o)$ is a delta function,

$$f(L-v_x(t-t_o)) = \delta[t_o-(t-\bar{t})], \quad \text{for} \quad t \geq \frac{L}{v_x} = \bar{t}$$

$$= 0, \quad \text{for} \quad t < \bar{t} \qquad 2.16$$

since no signal will have yet reached L. Thus, for $t \geq \bar{t}$,

$$i_a = -\frac{QI_o v_y}{\lambda y_c}[1-e^{-\lambda(t-\bar{t})}], \quad \text{for} \quad t_o < \frac{y_c}{v_y} = t_c ,$$
$$= -\frac{QI_o}{y_c}\frac{v_y}{\lambda}[e^{\lambda t_c}-1]e^{-\lambda(t-\bar{t})}, \quad \text{for} \quad t_o \geq t_c . \qquad 2.17$$

which is just $i_p(t_o)$ except that it is delayed by the time $\bar{t}$ necessary for the electrons to travel down the dynode strip.

In reality, it would be impossible to know exactly the functional form of $f(x-x_o)$, and, therefore, it is necessary to approximate it. Before beginning the discussion with a specific assumed form for $f(x-x_o)$, it is useful to show that as long as $f(x-x_o)$ is of finite extent the anode current will, after a sufficiently long time, decay exponentially with decay constant λ. For times longer than that required for the initial build-up of the anode current, that is,

$$t \geq \bar{t} + t_c + \tau , \qquad 2.18$$

where τ is the halfwidth of $f(x-x_o)$ at the anode, the limits of the integral over t_o will be determined as follows. The minimum value of t_o will be due to a pulse centered at a distance $v_x\tau$ past L. That is, for this pulse

$$x_o = L + v_x\tau = v_x(t-t_o^{min}) , \qquad 2.19$$

or

$$t_o^{min} = t - \bar{t} - \tau \,. \qquad 2.20$$

Likewise,

$$t_o^{max} = t - \bar{t} + \tau \,. \qquad 2.21$$

Making the substitution that

$$\alpha = t_o - (t-\bar{t}) \,, \qquad 2.22$$

the equation for the anode current becomes

$$i_a(t) = Ae^{-\lambda(t-\bar{t})} \int_{-\tau}^{\tau} f(\alpha) e^{-\lambda\alpha} \, d\alpha \,. \qquad 2.23$$

Thus, for any form of $f(\alpha)$ the integral is a constant, and i_a decays with the decay constant λ. With the assurance that after some time the measured decay will be the proper one, let us investigate in detail some approximate forms for $f(x-x_o)$.

As a first approximation, let $f(x-x_o)$ have the form

$$f(x-x_o) = e^{\gamma(t-t_o)}$$

$$= 0 \,, \qquad \text{for} \quad |x - v_x(t-t_o)| > \Delta(x_o) \,, \qquad 2.24$$

where

$$\Delta(x_o) = \Delta_o \frac{x_o}{L} = \Delta_o \left(\frac{t-t_o}{\bar{t}}\right) \,. \qquad 2.25$$

This form for $f(x-x_o)$ assumes that the electron pulse is an exponentially increasing square pulse that is spreading linearly in time. In order to identify the pulses which contribute to the anode current at a given time, it is necessary to examine two pulses which differ as follows. The earliest possible pulse that could contribute is one that is centered a distance $\Delta(x_2)$ past L at x_2. That is,

$$x_2 = L + \Delta(x_2) = L + \Delta_o \frac{x_2}{L} = L + \Delta_o \frac{v_x}{L}(t-t_o^{min})$$

$$= v_x(t-t_o^{min}) \quad . \qquad 2.26$$

Dividing by v_x, recalling that $\frac{L}{v_x} = \bar{t}$, and solving for t_o^{min}, we get

$$t_o^{min} = t - \left(\frac{1}{1-\frac{\Delta_o}{L}}\right)\bar{t} \quad . \qquad 2.27$$

By expanding the term

$$\left(1-\frac{\Delta_o}{L}\right)^{-1}, \qquad 2.28$$

t_o^{min} becomes

$$t_o^{min} = t - (1+\frac{\Delta_o}{L}+(\frac{\Delta_o}{L})^2+\ldots)\bar{t} \quad . \qquad 2.29$$

Since the width of an individual anode pulse is specified (by the Bendix Corporation) to be typically 3 nsec, it is reasonable to assume that,

at most, $\frac{\Delta_o}{L} = 0.1$. Thus, all terms of higher order than $\frac{\Delta_o}{L}$ can safely be neglected, leaving

$$t_o^{min} \tilde{=} t - \bar{t} - \tau \,, \qquad 2.30$$

where

$$\tau = \frac{\Delta_o \bar{t}}{L} = \frac{\Delta(L)}{v_x} \,. \qquad 2.31$$

A similar analysis for t_o^{max} gives

$$t_o^{max} \tilde{=} t - \bar{t} + \tau \,. \qquad 2.32$$

Thus, the spreading of the electron pulse during the time when the pulse can contribute to the anode current is so small that it can be neglected. Assuming that the time for an electron to move across the cathode is less than 2τ, there are five time intervals which must be examined:

i) $t < \bar{t} - \tau$,

and $i_a(t) = 0$.

ii) $\bar{t} - \tau \leq t \leq \bar{t} + \tau$, $\quad 0 \leq t_o \leq 2\tau$,

and $i_a(t) = \int_0^{t-\bar{t}+\tau} f(x-x_o) i_p(t_o < t_c) dt_o \,.$

iii) $\bar{t} + \tau \leq t \leq \bar{t} + t_c - \tau$, $\quad t - \bar{t} - \tau \leq t_o \leq t_c$,

and $i_a(t) = \int_{t-\bar{t}-\tau}^{t-\bar{t}+\tau} f(x-x_o) i_p(t_o < t_c) dt_o \,.$

iv) $\bar{t} + t_c - \tau \leq t \leq \bar{t} + t_c + \tau, \quad t - \bar{t} - \tau \leq t_o \leq t - \bar{t} + \tau,$

$$\text{and} \quad i_a(t) = \int_{t-\bar{t}-\tau}^{t_c} f(x-x_o) i_p(t_o < t_c) dt_o + \int_{t_c}^{t-\bar{t}-\tau} f(x-x_o) i_p(t_o \geq t_c) dt_o .$$

v) $\bar{t} + t_c + \tau \leq t, \quad t_c \leq t_o ,$

$$\text{and} \quad i_a(t) = \int_{t-\bar{t}-\tau}^{t-\bar{t}+\tau} f(x-x_o) i_p(t_o \geq t_c) dt_o . \qquad 2.33$$

In the first time interval no electron pulse has had time to reach the point L yet and thus $i_a = 0$. During the second time interval t_o^{min} will always be 0, because a full pulse width has not had time to move past L. Likewise, t_o^{max} will be determined by the pulse centered at $x_1 = L - \Delta(L)$. To determine the relationship between t and t_o^{max}, we use the equation

$$v_x(t - t_o^{max}) = L - \Delta(L) . \qquad 2.34$$

Dividing by v_x, and recalling $\frac{L}{v_x} = \bar{t}$ and $\frac{\Delta(L)}{v_x} = \tau$,

$$t = t_o^{max} + \bar{t} - \tau . \qquad 2.35$$

Substituting this value of t in the inequality for t in the second time interval, the following inequality for t_o^{max} is obtained:

$$0 \leq t_o^{max} \leq 2\tau . \qquad 2.36$$

Since t_o is always less than t_c in this time interval, the

functional form $i_p(t_o < t_c)$ must be used in the integral for i_a. Using a similar procedure, the several sets of inequalities occurring in the five time intervals can be determined. Using the values calculated earlier for $\bar{t}$ and t_c, a value of 1.5×10^{-9} sec for τ, a value of $0.875 \times 10^{9}\,\text{sec}^{-1}$ for γ (corresponding to a total gain of about 10^6), and a value of $(3.8 \times 10^{-9}\,\text{sec}^{-1})$ for λ, $i_a(t)$ has been calculated and is shown in Figure 9. At a time 20.6×10^{-9} sec after the exponentially decaying light signal is incident upon the cathode, the signal at L also shows an exponential decay with decay constant λ.

The problem was tried again using a gaussian function for the pulse shape, which would be a more realistic form. However, the effects of a spreading gaussian pulse become too difficult to treat. The form for $f(x-x_o)$ was

$$f(x-x_o) = e^{\frac{\gamma x_o}{v_x}} e^{-\left(\frac{x-x_o}{\Delta}\right)^2}, \qquad 2.37$$

where the first term accounts for the multiplication of the signal and the second term, the width of the electron pulse. The time intervals of interest here are

i) $0 \leq t < t_c$

where $i_a = \int_0^t i_p(t_o < t_c) f(x-x_o)\,dt_o$

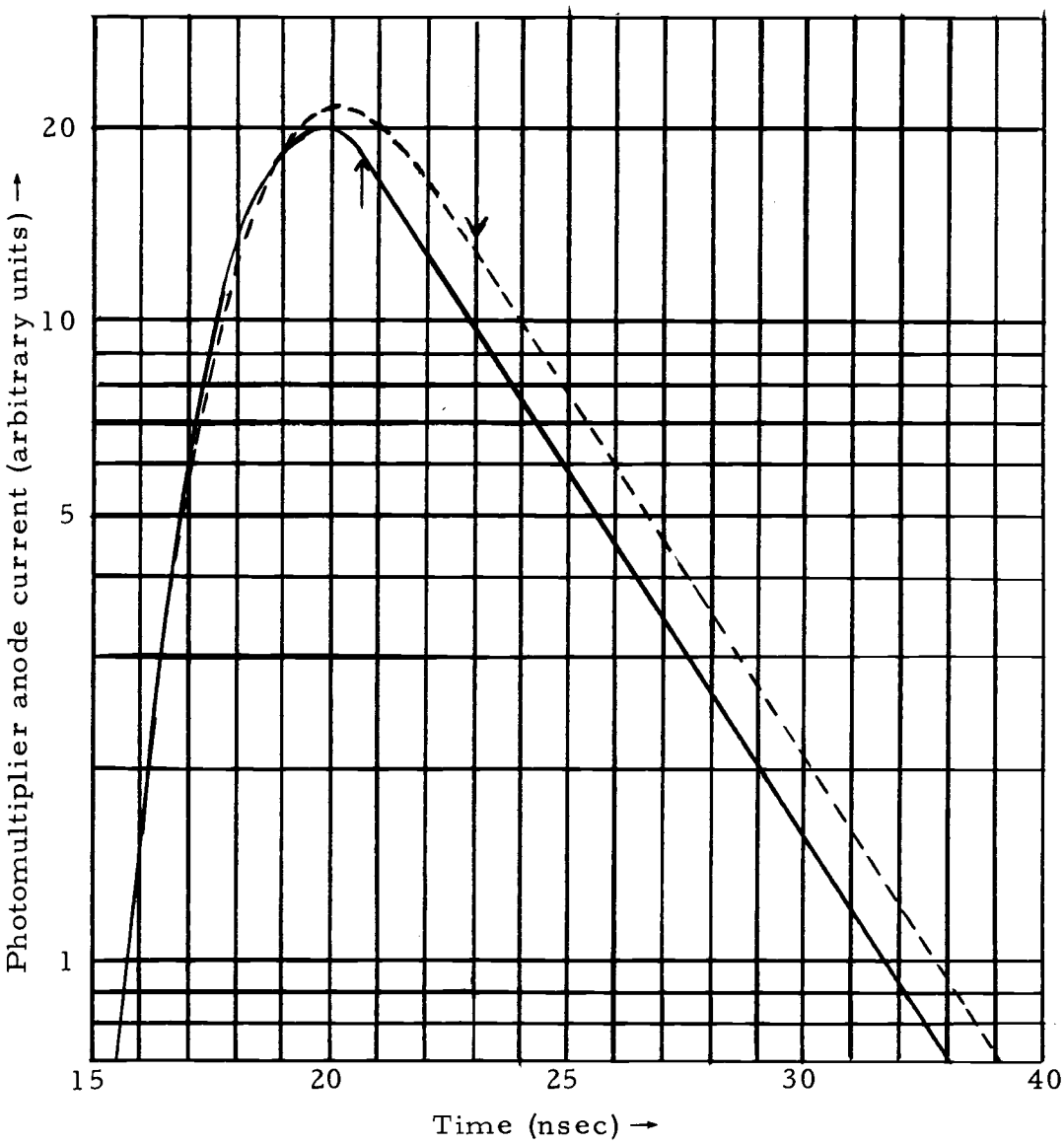

Figure 9. Time dependence of the photomultiplier anode current for an exponentially decaying light signal incident at t = 0. For the solid curve, a rectangular-shaped secondary electron pulse is assumed; the arrow in the figure depicts the time after which the anode current decays exponentially. For the dotted curve, a gaussian shaped pulse is assumed; the arrow depicts the time after which the anode current differs by less than 1% from an exponential decay.

ii) $t_c \leq t$

$$\text{where} \quad i_a = \int_0^{t_c} i_p(t_o < t_c) f(x-x_o)dt_o + \int_{t_c}^{t} i_p(t_o \geq t_c) f(x-x_o)dt_o \,. \qquad 2.38$$

These integrals can be evaluated in terms of error functions. A short computer program was written to evaluate $i_a(t)$, and these results are also shown in Figure 9. At a value of 23×10^{-9} sec the decay curve varies less than 1.0% from a true exponential with decay constant λ. The reason that the gaussian pulse shape takes a few nanoseconds longer to converge to an exponential is attributable to its broader extent. The important point, however, is that even with this pulse shape, which is of infinite extent, the signal at L converges to an exponential.

The final question that must be answered is the effect of sampling time on the measurement. As has been demonstrated, at some time after the light is incident upon the cathode, the signal at L becomes exponentially decreasing. The anode structure then samples this signal beginning at some time t_1 after the termination of the excitation. At this time the signal to be sampled is of the form

$$i_a(t) = Ae^{-\lambda t_1} e^{-\lambda \xi} . \qquad 2.39$$

where $t = t_1 + \xi$. If the response of the anode section is given by $g(\xi)$, then the charge collected at the anode during the interval ξ

to $\xi + d\xi$ is

$$dq = Ae^{-\lambda t_1} e^{-\lambda \xi} g(\xi) d\xi \ . \qquad 2.40$$

The total charge collected during the interval from t_1 to $t_1 + \Delta t$ is

$$q(t_1) = Ae^{-\lambda t_1} \int_0^{\Delta t} e^{-\lambda \xi} g(\xi) d\xi \ . \qquad 2.41$$

Thus, if Δt is held fixed, the detector output for a given delay time t_1 is proportional to the light intensity at that time. The quantity which is amplified is

$$i_a(t_1) = \frac{q(t_1)}{T} \ , \qquad 2.42$$

where T^{-1} is the repetition rate for the excitation. The decay curve is then reconstructed by changing the sampling time t_1.

In order to demonstrate the validity of the previous calculations, Figure 3 (page 20) shows a picture of the time relationship between the electron gun pulse and the MEM sampling pulse where the electron gun pulse has been delayed 20. 0 nanoseconds. The minimum delay time, for which the light decay in the krypton experiment was found to be decaying exponentially, was about 19 nanoseconds, which includes the time needed to terminate the excitation. The fact that the calculated time is slightly longer is easily accounted for by a slight

change in the nominal values or estimates used. In general, the agreement is good and indicates that the length of time needed to terminate the excitation is, at most, 2 to 3 nanoseconds.

Amplification of the MEM Anode Current

The values used for the excitation repetition rate were in the range 0.5 to 5 MHz for both the argon and the krypton experiments. The repetition rate to be used for a given decay was dictated by the lengths of the excitation and sampling pulses and by the decay constant itself. The photomultiplier anode current, which typically ranges from 1 to 100 pA, is amplified by a Hewlett Packard Model 425A Electronic Ammeter. This particular amplifier was used because it has a very high ac rejection, which is necessary because of the slight ac coupling between the MEM anode and DS02. The ammeter output is then displayed on a Varian G 11A strip chart recorder, where three-place accuracy is obtained from the recordings by averaging the recorded signal at each delay time for about two minutes.

Photomultiplier Vacuum System

The photomultiplier vacuum system is pumped by an 8 liter per second Vac-Ion pump (trademark of Varian Vacuum) through a metallic vacuum line approximately 2 feet in length and containing two right angle bends; this long vacuum line is used to insure that the 4000 volt

discharge inside the pump does not affect the operation of the MEM. The system is pumped to a pressure of 2.0×10^{-7} Torr at the pump. Finally, the MEM views the excitation chamber through a cleaved crystalline lithium fluoride window of one mm thickness which separates the two vacuum systems. The one inch diameter window is held in place with vacuum grade epoxy which also forms the vacuum seal. The extreme ultraviolet transmission properties of lithium fluoride windows will be discussed in Chapter III.

APPLICATION TO THE NOBLE GASES

Argon

An energy-level diagram (34, p. 212) of the first excited multiplet in argon is shown in Figure 10. Within this multiplet the $^3P_0$ and $^3P_2$ states are metastable, and the $^3P_1$ and $^1P_1$ states both decay to the ground state by allowed transitions at 1067 Å and 1048 Å, respectively. The decay of the $^3P_1$ level was first studied by itself, in order to avoid the complexity of a two component decay scheme.

In order to observe only the natural decay of the $^3P_1$ state, several conditions must be met. First, it is necessary to excite only the $^3P_1$ state, or else discriminate against the light from the $^1P_1$ transition. Since the energy resolution of the electron gun is not good enough to provide excitation of the $^3P_1$ state alone, it was necessary to discriminate against the light from the $^1P_1$ state. It was found that a lithium fluoride window provided just this wavelength discrimination. The absorption coefficient for lithium fluoride is shown in Figure 11 (20). Both transitions are very near the ultraviolet cutoff for lithium fluoride, and, consequently, the greater absorption of the 1048 Å line is enough to discriminate effectively against it.

In order to determine the discrimination against the 1048 Å line by the lithium fluoride windows, an excitation chamber with identical dimensions was constructed to mount on a 1/2-meter grazing incidence

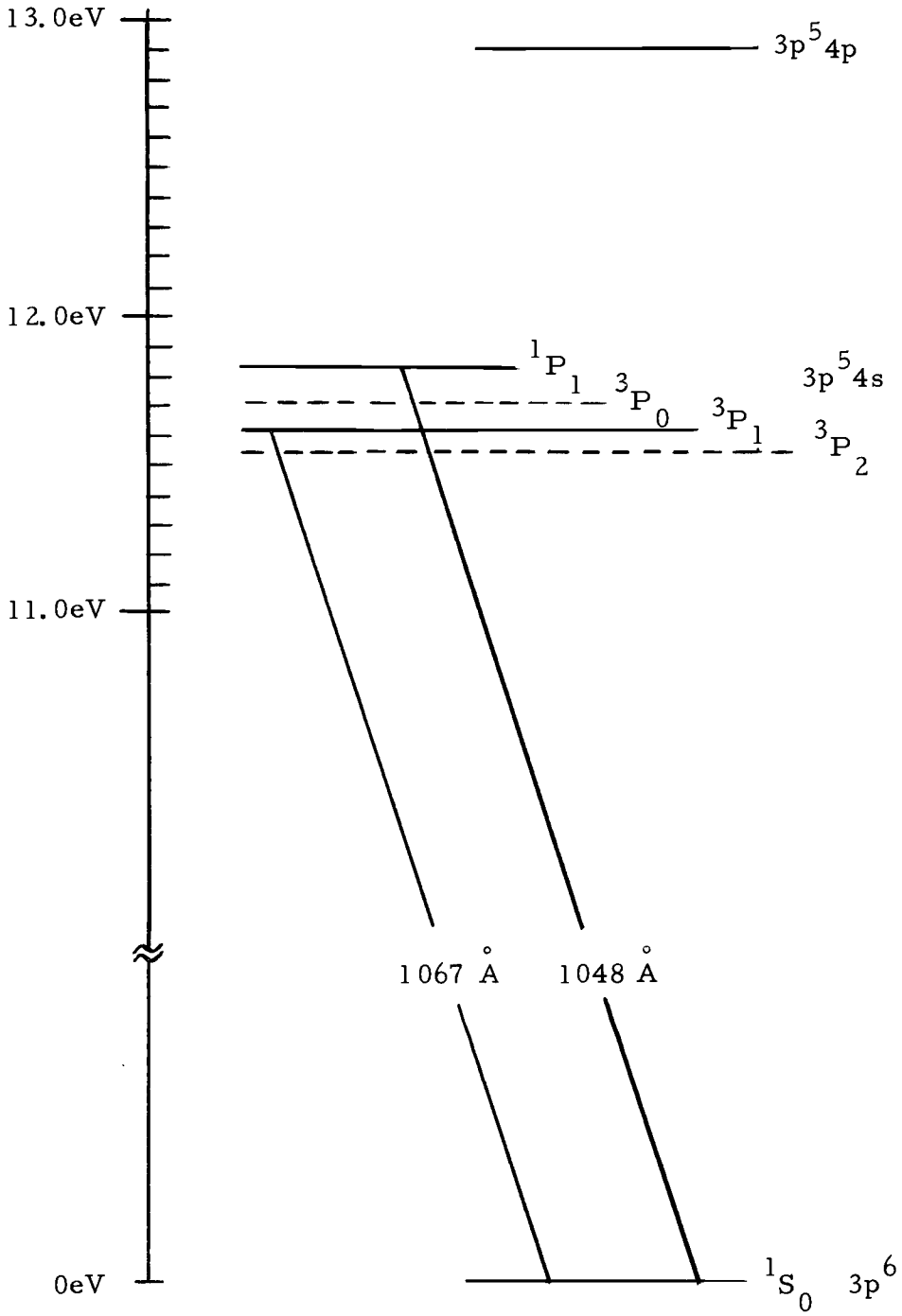

Figure 10. Partial energy-level diagram for argon.

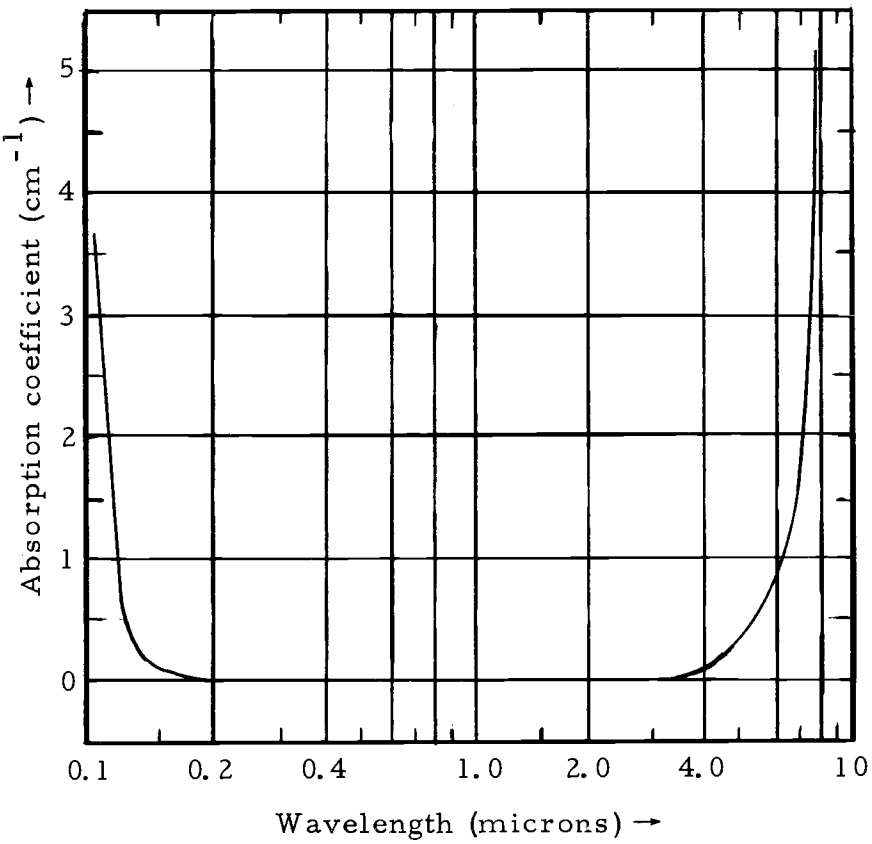

Figure 11. Wavelength dependence of the absorption coefficient of lithium fluoride.

vacuum spectrograph. When a 50 volt dc discharge in argon is viewed through a lithium fluoride window, no trace of the 1048 Å line is recorded while the 1067 Å line is clearly visible. However, when the lithium fluoride window is replaced by a 400 Å thick aluminum oxide (Al_2O_3) film (14), both lines are clearly visible. The thin films are made by anodizing ordinary aluminum foil in a solution of 22. 6 grams of ammonium citrate and 19. 2 grams of citric acid diluted in one liter of distilled water. The thickness of the Al_2O_3 film formed by this solution has been measured to be 13. 7 Å per volt of applied dc voltage. A drop, the size of the desired windows (3/8 to 1/2 inch), of sodium hydroxide is placed on the back side of the foil and left until it has removed the aluminum oxide film from that side. The foil is then immersed in an 18% HCl solution until the aluminum is eaten away, leaving a thin aluminum oxide film mounted on the remaining aluminum foil. After drying, the film is fastened with epoxy to a rigid holder. Although these films are quite fragile, it was found that those as thin as 400 Å could be mounted with reasonable success. The measured extreme ultraviolet transmission curve for a 420 Å thick film is shown in Figure 12. It was found that these films can support a pressure differential of about one Torr; thus they are suitable as a window between two vacuum systems only if the systems are evacuated together.

The bandpass of the detection system is thus determined by the high wavelength cutoff (1500 Å) of the MEM and the low wavelength

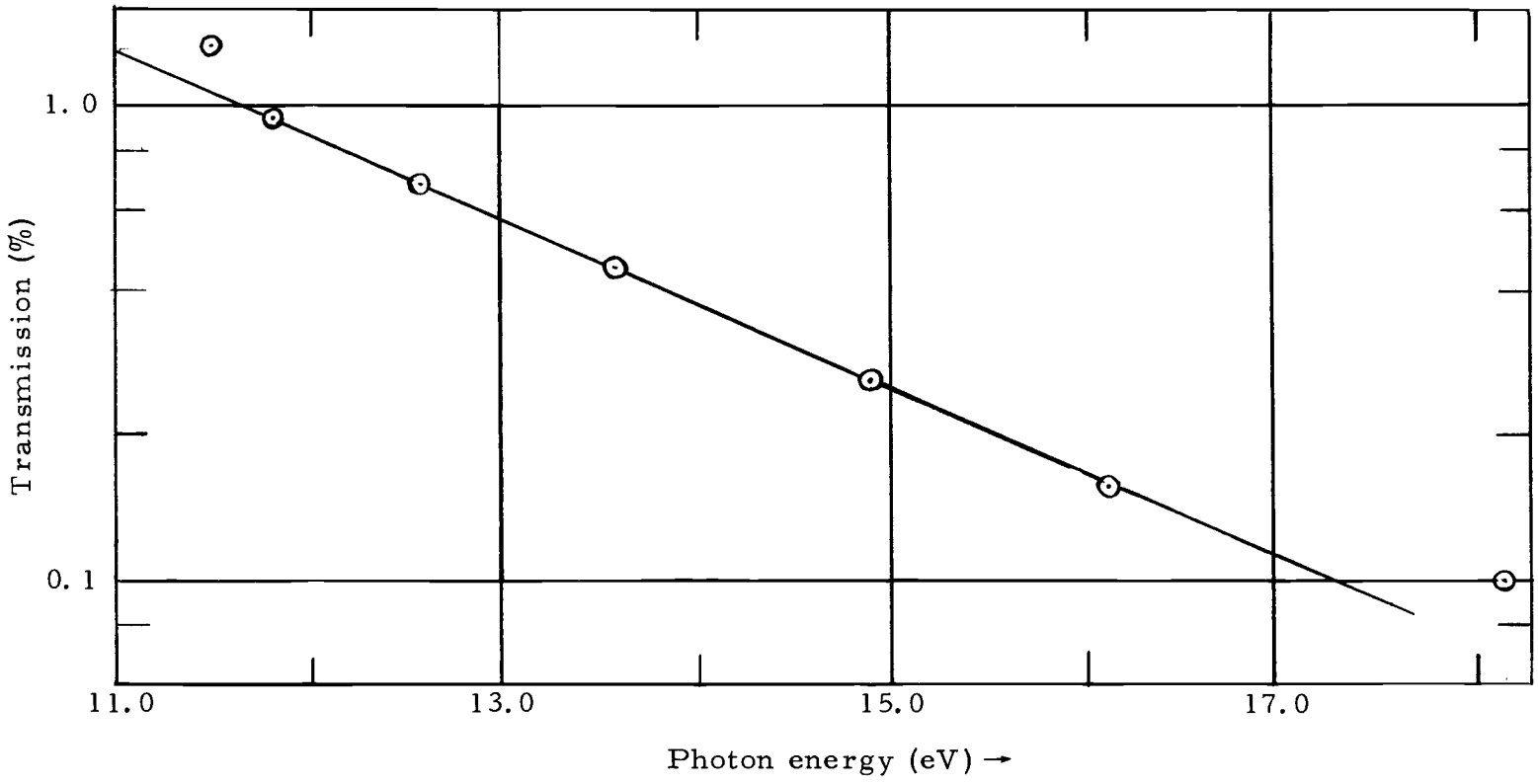

Figure 12. Transmission of a 420 Å thick aluminum oxide film as a function of photon energy.

cutoff (1050 Å) of the lithium fluoride window. Since all intermediate transitions in argon occur at wavelengths longer than 1500 Å, they are not observed. However, if higher levels are populated, some will decay to the first excited multiplet and thus alter the decay under study. In order to eliminate this cascading, a determination of the threshold for excitation of the $^3P_1$ state was made and is shown in Figure 13. The $^3P_1$ threshold occurs at about 13.5 volts, and, from the early part of the curve, the spread in energy of the bombarding electrons is estimated to be about 0.5 eV. The fact that the measured threshold occurs at about 1.9 volts above the transition energy for the $^3P_1$ resonance transition is probably due to a contact potential between the cathode material and the grid wires. The electron gun pulse was kept at 14.2 volts in order to obtain a usable signal and yet to minimize excitation of the $3p^5$ 4p levels. Qualitatively, the effect due to cascading only became apparent at electron gun voltages above 17.0 volts. Furthermore, the excitation pulse width was set at 20 nanoseconds to discriminate against the excitation of any of the long-lived $3p^5$ 4p and higher-lying levels (16) which might be excited.

The population of the $^3P_1$ state can also be affected by collision processes. For example, an atom in the $^3P_0$ metastable level might make a collision with a ground state atom, thereby exciting the ground state atom to the $^3P_1$ state. For this reason, the argon pressure was kept below 2×10^{-4} Torr in order to insure that such effects would be

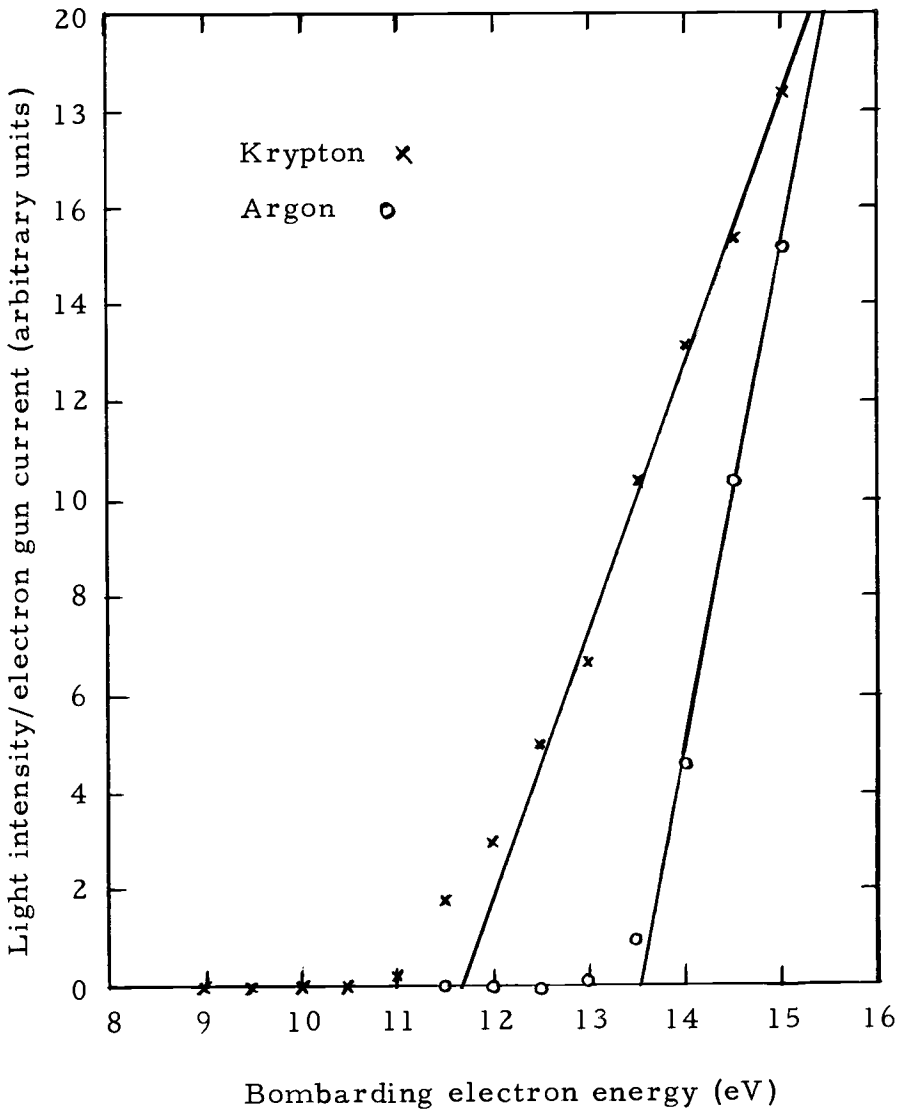

Figure 13. Threshold curves for excitation of the first excited J = 1 ($^3P_1$) levels in argon and krypton by electron bombardment.

negligible.

Finally, it is necessary to consider resonance trapping. This effect, which is discussed in detail in a later section, can be taken into account only by measuring the decay time as a function of argon pressure and extrapolating these measurements to zero pressure.

Two typical plots of photomultiplier current versus delay time are shown in Figure 14. The lower curve represents the decaying light signal from the system at background pressures, and the upper curve represents the sum of the lower curve and the signal due to argon. Although the origin of the background signal is unknown, it is possible that the background gas gives rise to several bands of molecular emission within the 1000-1500 Å bandpass of the detector. The decay curve for the background gas demonstrates the capability of the apparatus to measure a decay which is must faster than that due to argon.

To obtain the argon decay, the two curves of Figure 14 were subtracted, and then a least-squares fit was made to an exponential plus a constant by an iterative procedure on a CDC 3300 computer. This exponential decay is shown in Figure 15. The constant term is small in all cases, and is accounted for by a small argon signal due to electrons emitted from the electron gun filament and accelerated to the control grid. Other contributing factors may be a slight change in the transmission of the lithium fluoride window when argon is

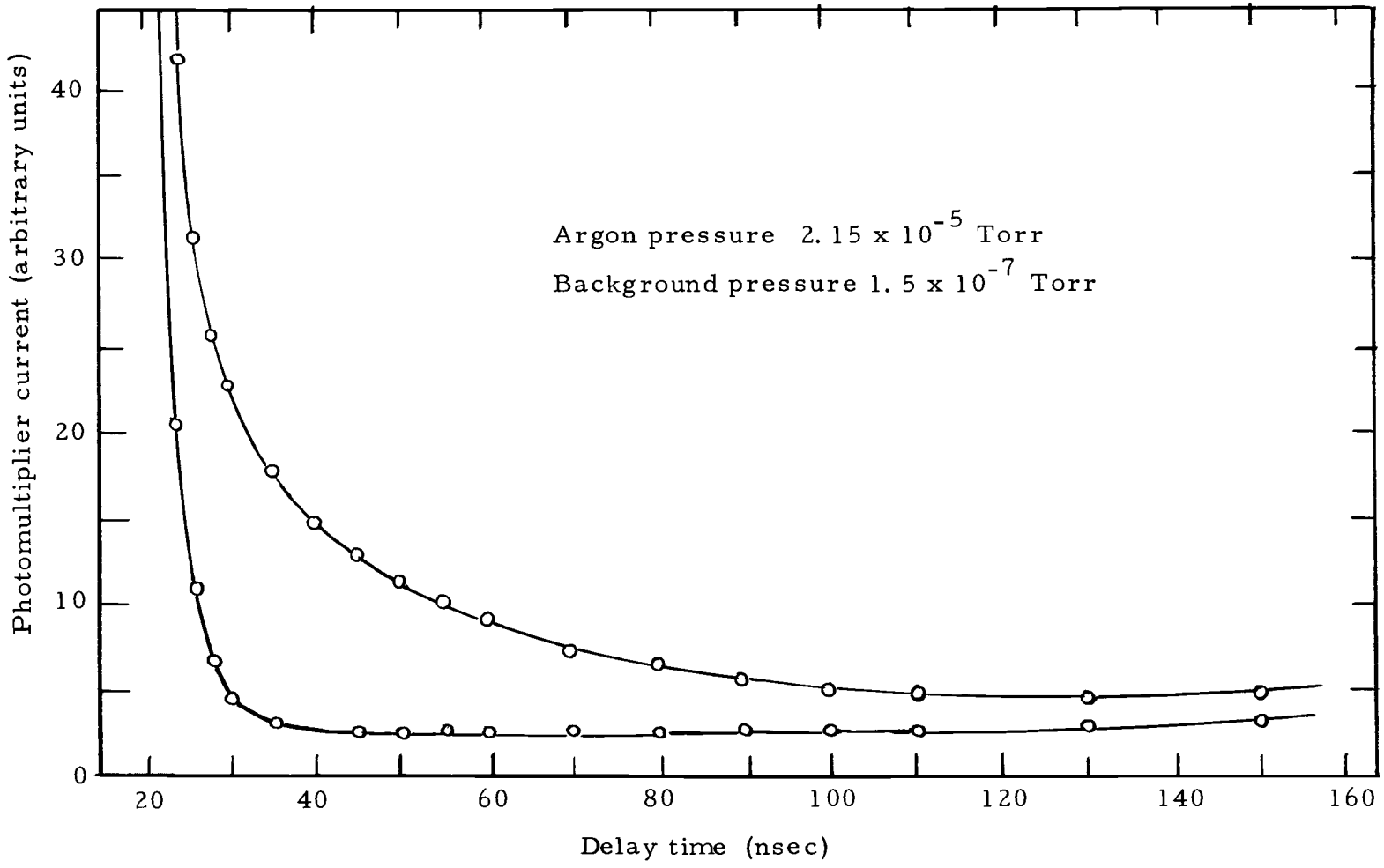

Figure 14. Typical plots of photomultiplier current as a function of delay time. The lower curve represents the decaying light signal from the system at background pressures and the upper curve represents the sum of the lower curve and the signal due to argon.

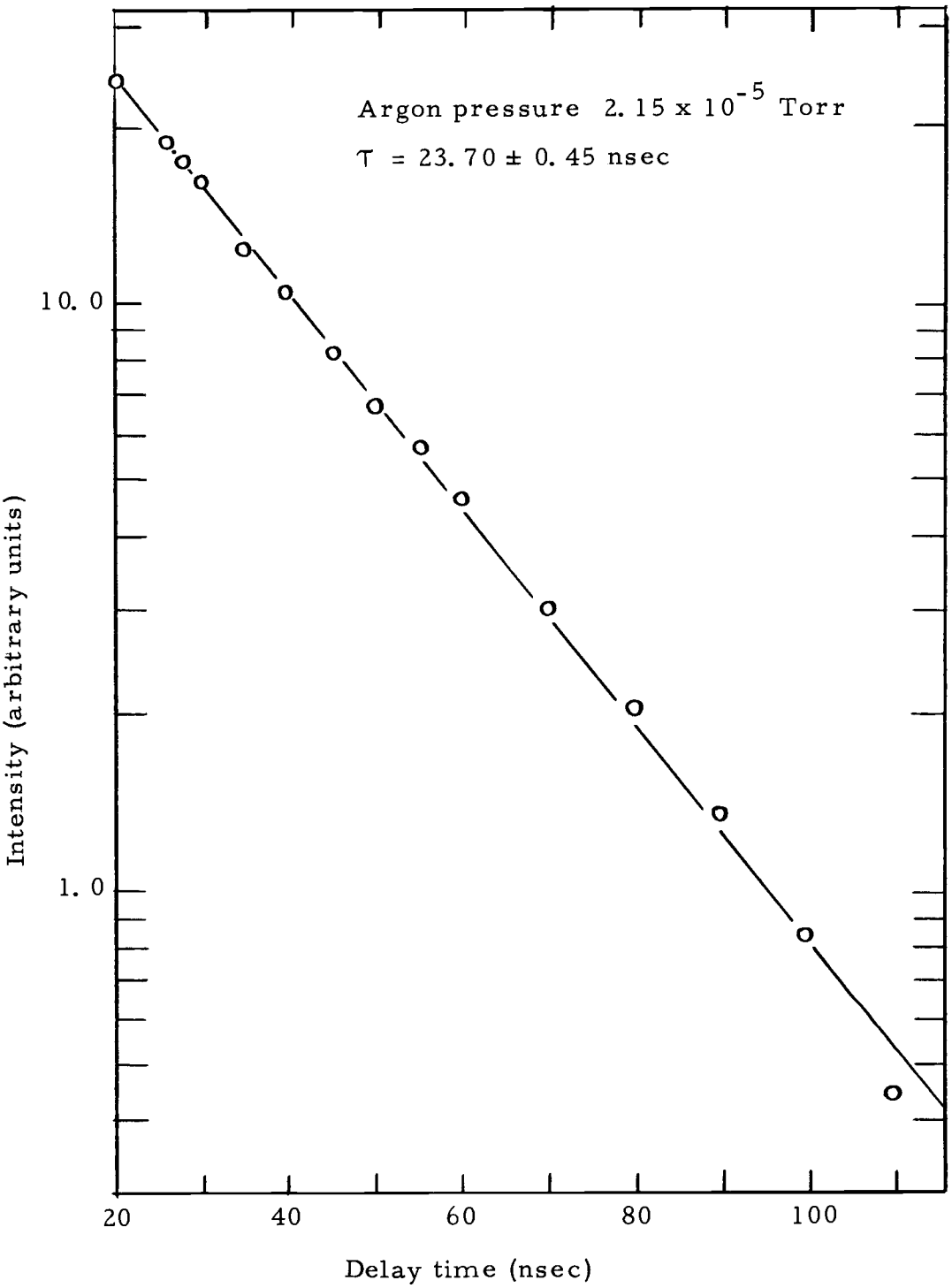

Figure 15. Typical argon-decay curve.

introduced into the system, or a higher background pressure when argon is admitted because of a decrease in the pumping speed for the system.

Lifetimes for the argon decay were measured in the pressure range from 5.0×10^{-6} to 2.0×10^{-4} Torr; these data are displayed in Figure 16. The lower limit of pressure was set by the minimum usable argon signal and, as discussed previously, the upper limit is low enough that the effects of collision processes upon the observed decays are negligible. Thus, the increase of lifetime with increasing argon pressure is attributed to resonance trapping, and a natural lifetime is obtained by extrapolating the measurements to zero pressure. The errors indicated in Figure 16 are standard errors of the mean of each least-squares fit, and they are approximately the same for all the points.

Krypton

An energy-level diagram (35, p. 170) of the first excited multiplet is shown in Figure 17. The $^3P_0$ and $^3P_2$ states are again metastable, while the $^1P_1$ and $^3P_1$ decay to the ground state by allowed transitions at 1165 Å and 1236 Å, respectively. Again, since these transitions are near the ultraviolet cutoff for lithium fluoride, it was hoped that the window would discriminate against the 1165 Å line. This discrimination was quantitatively examined, as in the case of

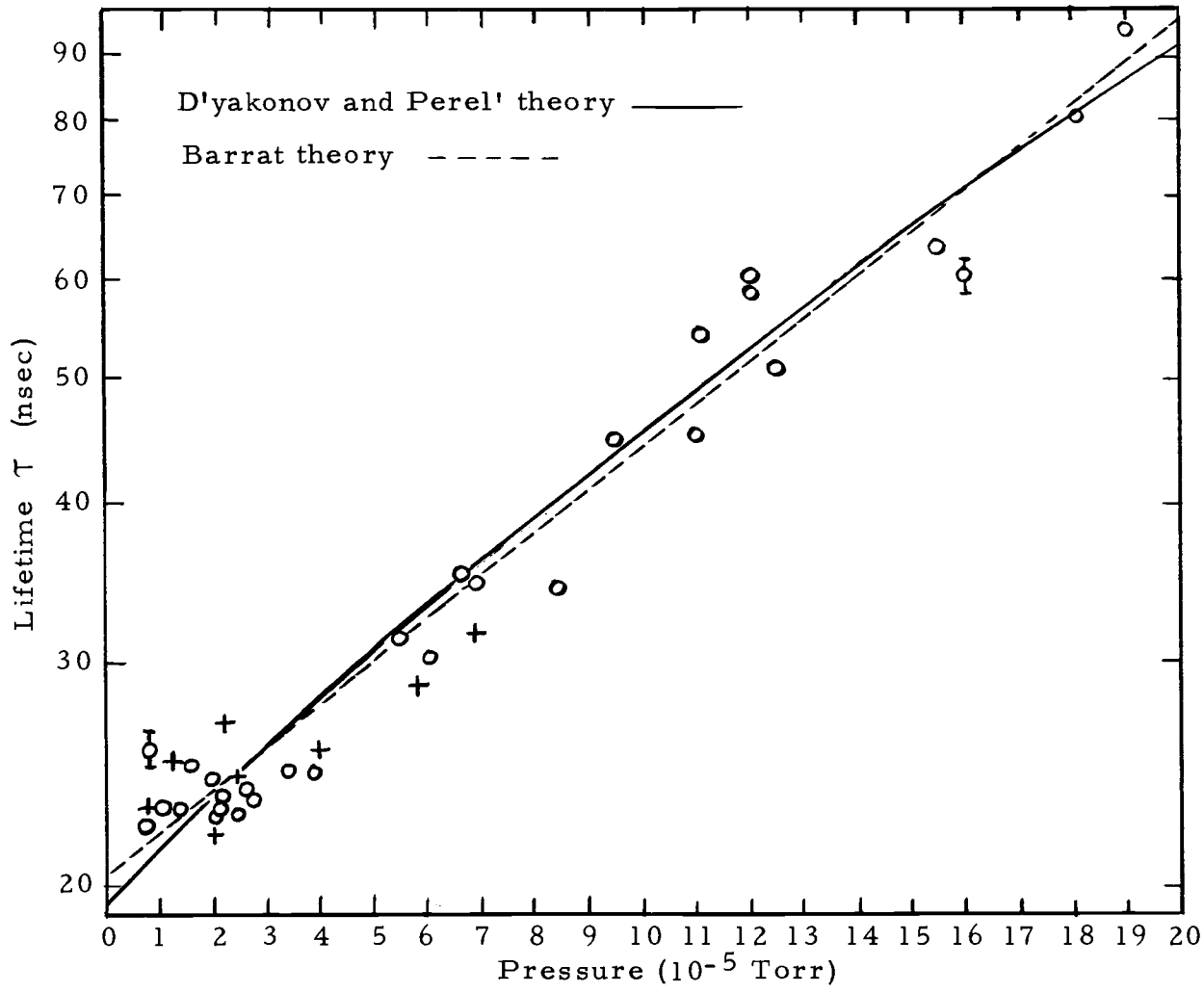

Figure 16. Imprisoned lifetime τ for the argon decay as a function of pressure. The open circles and crosses indicate data points taken with the center of the electron gun 3.5 and 2.0 cm, respectively, from the lithium fluoride window. Fits to the data taken at 3.5 cm are shown for the theories by Barrat, and D'yakonov and Perel'.

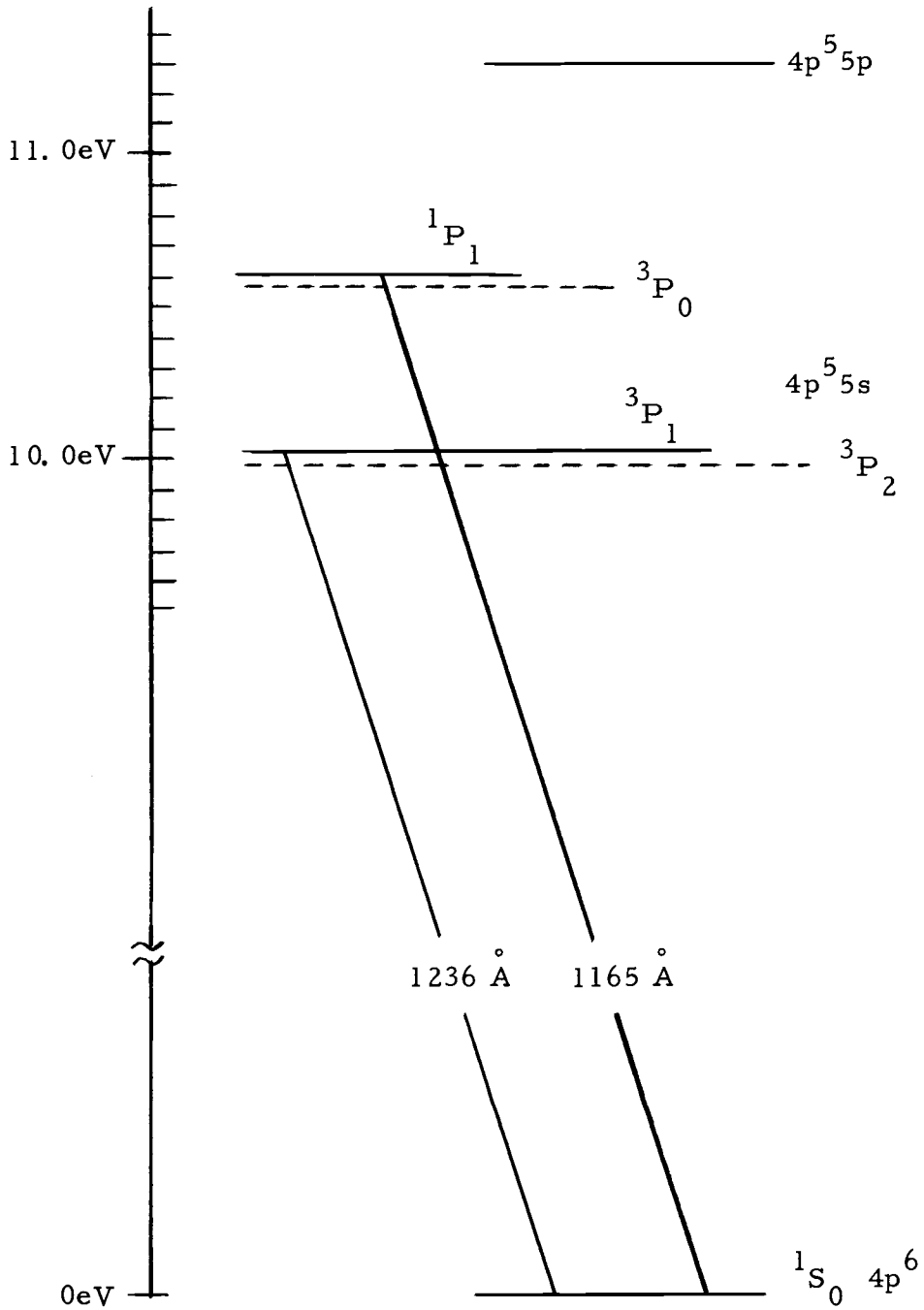

Figure 17. Partial energy-level diagram for krypton.

argon, with a 1/2-meter grazing incidence vacuum spectrograph. A 6SJ7 tube was used as an electron gun in the excitation chamber where a krypton discharge was set up by placing the control grid of the electron gun at +17. 0 volts with respect to the cathode. The photographs taken of the two transitions in the spectrograph gave the ratio of the intensity of the 1236 Å line to the 1165 Å line to be 6. 4. Therefore, it becomes necessary to provide further discrimination. Fortunately, the $^1P_1$ and $^3P_1$ levels lie 0. 56 eV apart, which means that the electron gun is capable of giving some added discrimination. The measured excitation threshold for krypton is also shown in Figure 13, and, as should be the case, this threshold lies approximately 1. 6 volts lower than that for argon. In order to obtain a usable signal, the electron gun pulse amplitude was raised to between 13. 5 and 14. 0 volts. This pulse has a length of about 6 nanoseconds, and, as is shown in Figure 3 (page 20), has an overshoot on the leading edge. It was this overshoot that was set at 13. 5 to 14. 0 volts, and thus the actual accelerating voltage was somewhat lower. The added discrimination provided by the electron gun is certainly enough to reduce the contribution of the $^1P_1$ resonance transition to below 10%, but this contribution will have to be taken into account in the absolute error associated with the measured lifetime of the $^3P_1$ level.

The krypton data were taken and analyzed in an analogous fashion to argon. The data for a typical run are displayed in Figures 18

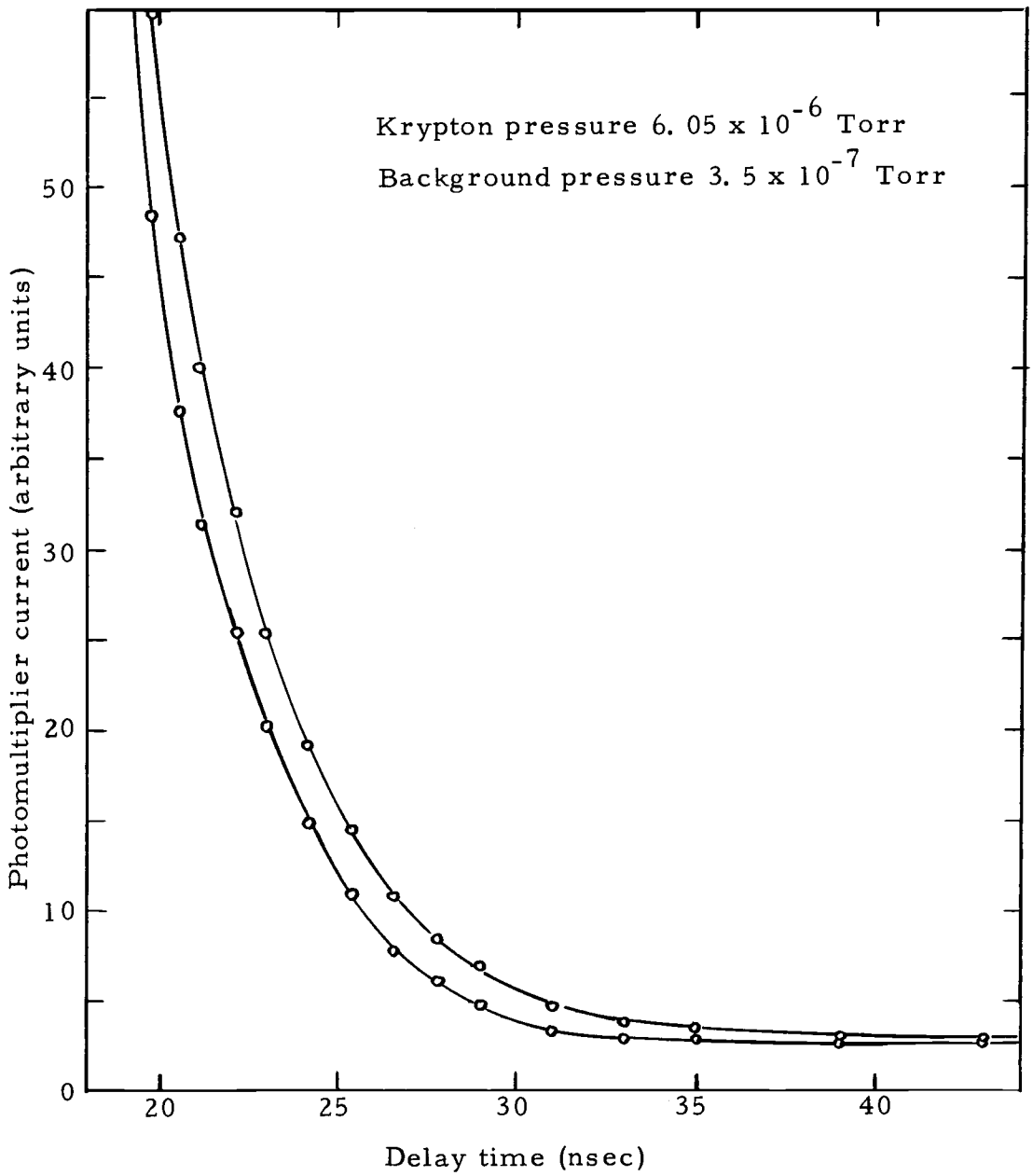

Figure 18. Typical plots of photomultiplier current as a function of delay time. The lower curve represents the decaying light signal from the system at background pressures and the upper curve represents the sum of the lower curve and the signal due to krypton.

and 19. The krypton decay was first studied in the pressure region from 0.6×10^{-6} to 25×10^{-6} Torr with the same electron gun configuration as the one used in argon. Later the electron gun was modified, as described earlier, to fit inside a 2.8 cm cylinder, and the measurements were extended to 45×10^{-6} Torr. The data from these runs are shown in Figures 20 and 21. Again the effects of resonance trapping are evident, and the interpretation of these data must be deferred until after this phenomenon is discussed in detail.

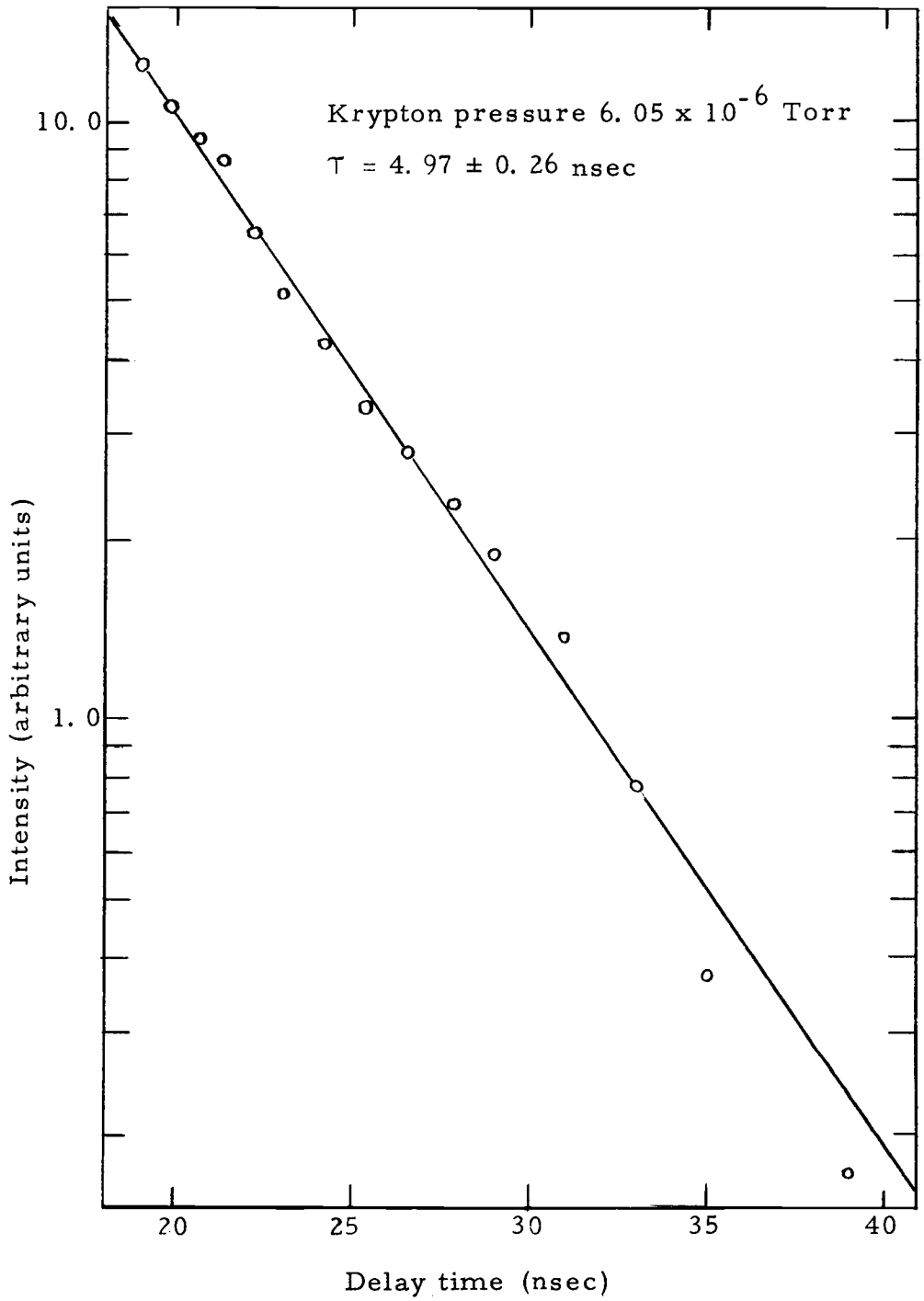

Figure 19. Typical krypton-decay curve.

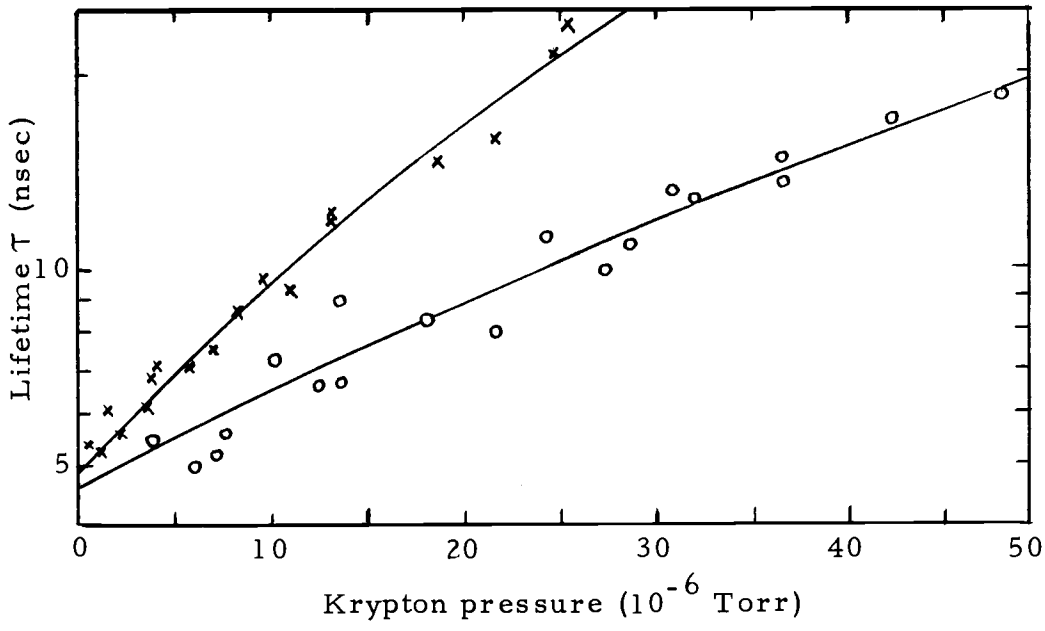

Figure 20. Imprisoned lifetime τ, for the krypton decay, as a function of pressure. The solid curve represents fit of the data to the theory of D'yakonov and Perel'. The excitation enclosure used for the lower set of data was considerably smaller than that used for the upper set of data.

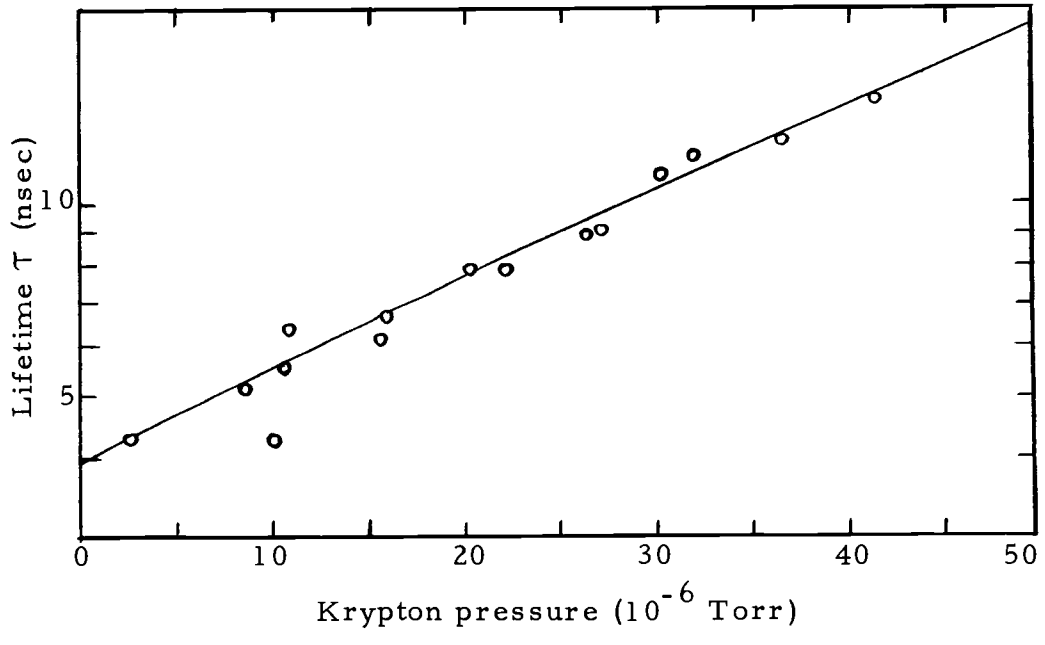

Figure 21. Imprisoned lifetime τ, for the krypton decay, as a function of pressure. The solid curve represents a fit of the data to the theory of D'yakonov and Perel'.

RESULTS AND CONCLUSIONS

Resonance Trapping

The initial theoretical development of the theory of resonance trapping was done by Milne (32) and Compton (10) using a kinetic theory approach where the diffusion of the photons toward the outside of the chamber was described in terms of a mean free path for the photons. The theory of Milne predicts that for a Doppler broadened line, the observed lifetime τ should increase with pressure according to the relation

$$\tau = \tau_o(1+Ap^2), \qquad 4.1$$

where τ_o is the natural lifetime, and

$$Ap^2 = \frac{4}{\pi^2} k_o^2[2L]^2, \qquad 4.2$$

where k_o is the absorption coefficient at the center of an absorption line (33, p. 100) and L is a chamber dimension.

In a more recent attempt to describe resonance trapping, Holstein (25, 26) has shown that it is incorrect to assume the existence of a mean free path for photons. An important feature of Holstein's theory is the determination of the probability, $T(\rho, \nu)$, that a photon of frequency ν will travel a distance ρ before being absorbed by the gas. For the case where a mean free path λ is assumed, the

expression for $T(\rho)$ is

$$T(\rho) = e^{-\rho/\lambda} \quad . \tag{4.3}$$

However, since the absorption coefficient $k(\nu)$ is a sensitive function of frequency, the monochromatic transmission factor $e^{-k(\nu)\rho}$ must be averaged over the frequency spectrum $P(\nu)$, of the radiation emitted from a given volume element. Thus, the probability that any photon will travel a distance ρ before being absorbed is

$$T(\rho) = \int_0^\infty P(\nu) e^{-k(\nu)\rho} d\nu \quad . \tag{4.4}$$

Holstein has shown that $k(\nu)$ is directly proportional to $P(\nu)$. For a doppler broadened line centered at ν_o,

$$k(\nu) = k_o e^{-\left[\frac{2(\nu-\nu_o)}{\Delta\nu_D}\sqrt{\ln 2}\right]^2} = \kappa\sqrt{\frac{\ln 2}{\pi}}\,\frac{2}{\Delta\nu_D}\,e^{-x^2} \tag{4.5}$$

where $\Delta\nu_D$ is the full width of the line at half maximum (33, p. 99), and κ is the constant of proportionality between $k(\nu)$ and $P(\nu)$. Substituting this value of $k(\nu)$ in the equation for $T(\rho)$, and changing the variable of integration from ν to x, we get

$$T(\rho) = \frac{1}{\pi^{1/2}} \int_{-\infty}^{\infty} e^{-x^2} e^{-k_o \rho\, e^{-x^2}} \, dx \quad , \tag{4.6}$$

where the lower limit has been extended from $-\frac{2\nu_o\sqrt{\ln 2}}{\Delta\nu_D}$ to $-\infty$. For optical transitions in gases near room temperature, the contribution to $T(\rho)$ from values of x such that

$$x < -\frac{2\nu_o\sqrt{\ln 2}}{\Delta\nu_D} \qquad 4.7$$

is negligible. In order to solve this integral for arbitary $k_o\rho$, it is necessary to resort to numerical integration. Holstein has developed solutions in closed form for $T(\rho)$ for several limiting situations; however, he has not treated the case of weak trappping where $k_o\rho$ is small. Since this case is the one of interest here, it will be examined later in more detail.

Once $T(\rho)$ has been evaluated, the equation for the transfer of radiation from one volume element to another can be formulated in terms of an integro-differential equation. Let $G(\vec{r}', \vec{r})d\vec{r}$ be the probability that a photon emitted at $\vec{r}'$ is absorbed in a volume element $d\vec{r}$ at $\vec{r}$. Denoting the concentration of excited atoms by $n(\vec{r}, t)$,

$$dt\, d\vec{r}\, \frac{\partial n(\vec{r}, t)}{\partial t} = a - b\,, \qquad 4.8$$

where a is the increase, due to absorption, and b is the decrease, due to emission, in the number of excited atoms in the volume element $d\vec{r}$ in a time dt. In this equation the diffusion of excited

atoms, which is negligible at room temperature, is neglected. Thus,

$$b = \gamma n(\vec{r}, t)\, d\vec{r}\, dt , \qquad 4.9$$

where γ is the probability for a decay of the atomic level of interest. However, to obtain a, all the volume elements $d\vec{r}'$ must be taken into account. The contribution from each volume element $d\vec{r}'$ in dt is just $\gamma n(\vec{r}', t)d\vec{r}'\, dt$ times the probability, $G(\vec{r}', \vec{r})d\vec{r}$, of a photon emitted at $\vec{r}'$ being absorbed in $d\vec{r}$. If all the volume elements $d\vec{r}'$ are considered, then

$$a = \gamma dt\, d\vec{r} \int_{\text{over enclosure}} n(\vec{r}', t)G(\vec{r}, \vec{r}')d\vec{r}' . \qquad 4.10$$

In this expression it is assumed that the time of flight for the photon is very much smaller than the lifetime of the state, and that the walls of the system are nonreflecting. Thus, the equation for the concentration of excited atoms becomes

$$\frac{\partial n(\vec{r}, t)}{\partial t} = -\gamma n(\vec{r}, t) + \gamma \int_{\text{over enclosure}} n(\vec{r}', t)G(\vec{r}, \vec{r}')d\vec{r}' . \qquad 4.11$$

There exist solutions to this equation of the type

$$n(\vec{r}, t) = n(\vec{r})e^{-\beta t} , \qquad 4.12$$

where $n(\vec{r})$ and β satisfy the equation

$$(1-\frac{\beta}{\gamma})n(\vec{r}) = \int_{\text{over enclosure}} n(\vec{r}\,')G(\vec{r},\vec{r}\,')d\vec{r}\,' . \qquad 4.13$$

Holstein shows that the relationship existing between $T(\rho)$ and $G(\vec{r},\vec{r}\,')$ is

$$G(\vec{r},\vec{r}\,') = -\frac{1}{4\pi\rho^2}\frac{\partial T(\rho)}{\partial \rho} \qquad 4.14$$

where $\rho = |\vec{r} - \vec{r}\,'|$. In principle, then, these equations may be solved for β. Indeed, Holstein gives the solution for a myriad of examples, except the one of interest here which is weak imprisonment of radiation having a Doppler line shape. As a first approximation, let the concentration of excited states be a constant throughout the volume. Additionally, the absorption volume available for each emitted photon will be assumed to be a sphere of radius L. For these approximations

$$1 - \frac{\beta}{\gamma} = -\int_0^L \frac{\partial T(\rho)}{\partial \rho} d\rho = -T(L) + T(0) , \qquad 4.15$$

where the value of $T(0)$ is just 1. Substituting the expression for $T(L)$, given by Equation 4.6, Equation 4.15 becomes

$$\frac{\beta}{\gamma} = \frac{\tau_o}{\tau} = \frac{1}{\pi^{1/2}}\int_{-\infty}^{\infty} e^{-x^2} \exp[-k_o L\, e^{-x^2}]dx . \qquad 4.16$$

where τ_o is the natural lifetime and τ is the observed lifetime.

Thus, a solution is obtained for weak trapping. However, as was mentioned earlier, numerical methods must be employed to solve it.

More recently there have been two attempts to describe resonance trapping, both from the quantum electrodynamic approach to resonance absorption (2, 3, 4, 15). This approach has the advantage over Holstein's method in that the effects of the polarization of optical and radio frequency perturbing fields, such as those present in level crossing (19) and double resonance experiments (9), can be explained. The details of these investigations will not be presented here; however, the pertinent results will be discussed in light of the approximations involved.

The first attempt using the quantum electrodynamic approach was given by Barrat, in which he assumed a single speed for all the atoms and a particular spatial relationship among the atoms. Barrat's results predict that for weak resonance trapping

$$\tau = \tau_o \exp\left(\left(\frac{\pi}{6}\right)^{1/2} k_o L \right). \qquad 4.17$$

The most recent attempt to describe resonance absorption is due to D'yakanov and Perel'. Their development is similar to that of Barrat's, except that they eliminate the single speed approximation by using the correct Boltzman velocity distribution for the atoms. For the case of Doppler broadened absorption and emission lines,

they obtain the result:

$$\frac{\tau_o}{\tau} = \frac{1}{\pi^{1/2}} \int_{-\infty}^{\infty} e^{-x^2} \exp[-k_o L e^{-x^2}] dx. \qquad 4.18$$

This is exactly the result obtained previously from Holstein's theory by assuming that the concentration of excited states was independent of position. For the case of weak trapping where $k_o L$ is small, this equation reduces to

$$\tau = \tau_o (1+(1/2)^{1/2} k_o L) , \qquad 4.19$$

and the results of Barrat reduce to

$$\tau = \tau_o (1+(\frac{\pi}{6})^{1/2} k_o L) . \qquad 4.20$$

Thus, for the case of very weak imprisonment, the theories of Barrat and D'yakonov and Perel' are essentially equivalent, whereas for the situation where $k_o L$ is not small, the results of D'yakonov and Perel' are exactly equivalent to those of Holstein's theory where the concentration of excited states is assumed to be uniform throughout the excitation chamber. For the case of heavy trapping where $k_o L$ is indeed very large, Holstein's solution of the problem in an infinite cylinder predicts a bell-shaped distribution of excited states with the concentration of excited states going to zero at the walls;

for this situation, his treatment agrees within a factor of order unity with the results of D'yakonov and Perel'.

Experimental Results

It now becomes possible to fit the measured lifetimes versus gas pressure data for argon and krypton with the theories of resonance trapping and to determine the lifetime at zero pressure, that is, the natural lifetime. Since resonance trapping was investigated more thoroughly during the krypton experiment than during the argon experiment, it is appropriate to discuss the krypton results first.

Three sets of data taken for the measured lifetime of the first excited J = 1 ($^3P_1$) level in krypton as a function of gas pressure are shown in Figure 20 and 21 along with a least squares fit to the D'yakonov and Perel' theory. A best fit to this theory was obtained by writing Equation 4. 18 in the form

$$\frac{1}{\tau} = \frac{1}{\tau_o} \sum_{n=0}^{\infty} \frac{(-k_o L)^n}{n!(n+1)^{1/2}} , \qquad 4.21$$

and, for each value of $k_o L$, terminating the series at the first term whose absolute value is less than 10^{-7}. These three sets of data were taken under the following conditions. The first set of data taken (upper set of data in Figure 20) was taken in the same manner as the data

taken in argon with the axis of the electron gun 3. 5 cm from the lithium fluoride window in the four liter excitation chamber. The best least squares fit to these data gives a value of 4. 87 ± 0. 26 nanoseconds for the natural lifetime and 5. 6 cm as the chamber dimension. Since the geometry of this excitation chamber was not perfectly cylindrical, and because the large size of the excitation chamber made it doubtful that the initial distribution of excited atoms was uniform, it was decided to better define the excitation region and to reduce the effects of resonance trapping by placing the electron gun in a stainless steel cylinder 2. 8 cm in diameter. Although the distribution of excited atoms is still unknown, it is certainly more nearly uniform in this smaller region, and, as can be seen in Figure 21, the effects of resonance trapping are greatly reduced. The natural lifetime determined from these data is 3. 89 ± 0. 17 nsec, and the best fit to the cylinder diameter is 2. 3 cm.

Each of the data points in Figures 20 and 21 represent the lifetime of a decay curve which was fit to a single exponential plus a constant. It was found that the constant term, which ranged to as high as 10% in a few cases, was reduced to below 2% by replacing the ac electron gun filament supply with a regulated negative dc supply. This seems to indicate that electrons accelerated by the filament wires were causing some excitation of the gas. The lower set of data in Figure 20 was taken with the negative dc voltage filament supply, and

gives a value of 4. 60 ± 0. 29 nsec for the natural lifetime and 2. 6 cm for the cylinder diameter. As can be seen in Figures 20 and 21, the theory of D'yakonov and Perel' fits the data well with a reasonable dimension for the size of the excitation chamber.

To the best of the author's knowledge, the data in Figures 20 and 21 represent the first experimental verification of the D'yakonov and Perel' theory. Furthermore, these data indicate that the often used (1, 4) Barrat theory, which is a straight line on this plot, is not adequate to describe the effects of resonance trapping over the pressure range of the present study. Likewise, the $\tau = \tau_o(1+Ap^2)$ dependence given by Milne's theory is easily seen to be incorrect as was pointed out by Holstein (25). The data for the large excitation chamber (upper curve in Figure 20) show the increased effects of resonance trapping, and indicate that this effect is properly accounted for by the D'yakonov and Perel' theory even though the initial distribution of excited atoms is most likely not uniform for this configuration.

Before a value of the lifetime can be determined, it is necessary to examine the possible sources of systematic errors. The 1% uncertainty in the sweep speeds of the oscilloscopes used to measure the sampling time is negligible compared to the scatter in the data of Figures 20 and 21. The 10% uncertainty in the absolute calibration of the pressure gauges can only give rise to a systematic change in the value of the excitation chamber dimension L, determined by the

least squares fit of the resonance trapping theories to the data, and therefore will not affect the value for the natural lifetime. The output pulse shape from both E-H Model 120D pulse generators was found to depend slightly upon the shape and duration of their trigger pulses. A careful check was made periodically to insure that neither the electron gun pulse or the photomultiplier gating pulse varied in time or with the delay time between these pulses. Another source of systematic errors would be a nonlinearity in the detection system. The linearity of the dc amplifier and recorder was checked periodically to within 1% using a Southwestern Industrial Electronics Model K-1 Microsource. For the photomultiplier itself, the measured signals were so small that any nonlinearity due to the depletion of charge from the dynode strip is negligible.

Finally, it must be remembered that perhaps as much as 10% of the krypton signal is due to light from the $^1P_1$ transition coming through the lithium fluoride window. Both the measurement of Wilkinson (42) and the calculation by Dow and Knox (13) indicate that this lifetime is very nearly the same as that of the $^3P_1$ level. Thus, there is no hope of separating the two decays, and the errors associated with the $^3P_1$ lifetime must reflect this uncertainty.

Using the average value of the intercepts of the curves in Figures 20 and 21, a value of 4.5 ± 0.6 nsec is given as the natural lifetime of the $(4p^5 5s)\ ^3P_1$ transition in krypton. Table 1 gives a short

resumé of the lifetime measurements for the first excited multiplet in argon and krypton. The value obtained from the present experiment agrees well with the indirect lifetime measurements that have been made, and it also agrees well with the value calculated by Dow and Knox. Since this measurement can be compared with the results of two other independent experiments, it serves to check the experimental setup and technique for unforeseen systematic errors.

Table 1. Lifetime determinations in argon and krypton.

Lifetimes (nsec)		Author	Method
$^3P_1$	$^1P_1$		
Krypton			
4.15		Turner (41)	Saturated resonance trapping
4.38	4.55	Wilkinson (42)	Resonance absorption
4.5 ± 0.6		Present study	Modified delayed coincidence
4.51	4.00	Dow and Knox (13)	Calculation
Argon			
19.3 ± 1.5		Present study	Modified delayed coincidence
10.2 ± 40%	2.5 ± 20%	Knox (29)	Calculation

The experiment in argon constitutes the first lifetime measurements for a resonance transition in this atom. The data for this experiment are shown in Figure 16 along with a least squares fit to both the Barrat and the D'yakonov and Perel' theories, because the data

are not good enough to distinguish between the theories. The scatter in the data was larger in this experiment because, as was discussed earlier, the experimental technique was not as good as it was for the krypton experiment. A fit to the Barrat theory gives 20. 3 ± 0. 7 nsec for the natural lifetime and a chamber diameter of 4. 2 cm, while the D'yakonov and Perel' theory gives 19. 3 ± 0. 9 nsec for the natural lifetime and 4. 9 cm for the chamber diameter. Probably neither of the curve fits to the data is as reliable as the errors given, because the initial (t = 0) spatial distribution of excited atoms in the excitation chamber may have varied with pressure. However, as the experiment in krypton has shown, the description given by the theory of D'yakonov and Perel' is the less approximate of the two; thus, a value of 19. 3 ± 1. 5 nsec is given as the value for the natural lifetime of the $(3p^5 4s)\ ^3P_1$ level in argon. As shown in Table 1, this value does not agree with the lifetime of 10. 2 ± 40% calculated by Knox. In order to determine the significance of this discrepancy, it is useful to briefly review the method of calculation.

Lifetime Calculations

The first excited multiplet and ground state in both argon and krypton have been investigated theoretically (13, 22, 29) and wave functions for both have been calculated using the Hartree-Fock method (11, 21, 39, 40). The complete details of these calculations are too

involved to be treated here; however, a short discussion of the method serves as a reminder of the approximations that are made.

The problem to be solved is to find the wave function ψ for an N electron atom which satisfies Schrödinger's equation,

$$H\psi = E\psi \, . \qquad 4.22$$

The approximation that has been most often used as a starting point is to regard each electron as being in a stationary state in the field of the nucleus and of the other electrons. This means that ψ can be written as

$$\psi = u_1(1)u_2(2)\ldots u_N(N) \, , \qquad 4.23$$

where the u's are single electron wave functions, each assumed to be the product of a function of coordinates and a function of spin. The subscript denotes the various single electron wave functions, and the label in parentheses indicates the individual electrons. This wave function, a product of spin-orbitals, is still not adequate because it does not satisfy the Pauli exclusion principle; the wave function must be antisymmetric upon the interchange of any two electrons. This principle can be satisfied by forming a determinantal wave function of the form

$$\psi = (N!)^{-1/2} \begin{vmatrix} u_1(1)u_1(2) \ldots u_1(N) \\ u_2(1)u_2(2) \ldots u_2(N) \\ \ldots \quad \ldots \quad \ldots \quad \ldots \\ u_N(1)u_N(2) \ldots u_N(N) \end{vmatrix} . \qquad 4.24$$

It has been assumed here that all spin-orbitals corresponding to the same values of m_s are orthogonal to each other, while those corresponding to different values of m_s are orthogonal because of the spin functions. Furthermore, all the spin-orbitals are assumed to be normalized.

The next problem is to determine what terms in the Hamiltonian give the major contribution to the energy, and yet can still be handled mathematically. The usual procedure is to neglect magnetic interactions entirely and approximate the Hamiltonian by (using Hartree atomic units)

$$H = \sum_{i=1}^{N} - \nabla_i^2 - \frac{2Z}{r_i} + \sum_{i>j} \frac{2}{r_{ij}} , \qquad 4.25$$

where the first term is the sum of the kinetic energies of the N electrons, the second is the potential energy of the N electrons in the field of the nucleus, r_i being the distance from the nucleus to the i^{th} electron, and the last term is the sum of the repulsive Coulomb potential energies between electrons, where r_{ij} is the distance

between the i^{th} and j^{th} electrons. In the case of the gound state of krypton and argon, Equation 4. 25 is an especially good approximation because these atoms consist only of electrons in filled shells. For this case it can be shown that the contribution of the magnetic interactions summed over all the electrons is zero.

The energy for the system in this approximation is just

$$E' = \int \psi^* H \psi d\tau \ . \qquad 4.26$$

In order to derive the Hartree-Fock equations, we now wish to vary the u_i's in order to minimize E', maintaining the subsidiary conditions that all the u_i's are normalized and that any two of the u_i's associated with the same m_s are orthogonal. These conditions can be imposed by the use of undetermined multipliers, by demanding that

$$\delta \left\{ E' + \sum_i \lambda_{ii} \int u_i^*(1) u_i(1) d\tau_1 \right.$$

$$\left. + \sum_{i>j} \delta(m_{si} m_{sj}) \left[\lambda_{ij} \int u_i^*(1) u_j(1) d\tau_1 + \lambda_{ji} \int u_j^*(1) u_i(1) d\tau_1 \right] \right\} = 0. \qquad 4.27$$

The term $\delta(m_{si} m_{sj})$ is one if $m_{si} = m_{sj}$, and zero otherwise. Carrying out the variation leads directly to the Hartree-Fock equations:

$$- \nabla_1^2 u_i(1) - \frac{2Z}{r_i} u_i(1) + \left[\sum_{j=1}^{N} \int u_j^*(2) \left(\frac{2}{r_{1,2}} \right) u_j(2) d\tau_2 \right] u_i(1)$$

$$- \left[\frac{\sum_{j=1}^{N} \delta(m_{si} m_{sj}) \int u_i^*(1) u_j^*(2) (2/r_{ij}) u_j(1) u_i(2) d\tau_2}{u_i^*(1) u_i(1)} \right] u_i(1) = \epsilon_i u_i(1) , \qquad 4.28$$

where $\epsilon_i = -\lambda_{ii}$. Equation 4.28 may be interpreted as the wave equation for a single particle wave function u_i. The Hamiltonian operator is the sum of the kinetic energy, the potential energy in the field of the nucleus of charge Z, and the potential energy in the field of N electrons distributed in the orbitals occupied in the determinantal wave function minus a correction term which is called the exchange term. This last term comes from the requirement that the wave functions must be antisymmetric. Clearly the electron cannot exert a Coulomb interaction on itself, so the exchange term must make a correction for this included term. The exchange term can be regarded as representing the potential energy at point 1 of the electron in question, due to a charge distribution at point 2 with the magnitude

$$\sum_j \delta(m_{si} m_{sj}) \frac{u_i^*(1) u_j^*(2) u_j(1) u_i(2)}{u_i^*(1) u_i(1)} . \qquad 4.29$$

This term will be called the exchange charge density. The total

charge from this term is just one, as can be seen by integrating the exchange charge density over $d\tau_2$. Since all of the u_i's are orthogonal, only the one term $j=i$ in the sum contributes, giving one charge. Furthermore, the exchange charge density consists of only electronic charge with the same spin as the one in question because of the multiplication by $\delta(m_{si}m_{sj})$. If we let point 1 and point 2 coincide, the exchange charge density becomes

$$\sum_j \delta(m_{si}m_{sj})u_j^*(1)u_j(1), \qquad 4.30$$

or the total density of all electrons of the same spin as the one in question at the point 1. These properties let us interpret the exchange term. The potential energy of the electron in question is due to the nucleus, to all the electrons with spin different than the one considered, and to all the electrons with the same spin as the one in question except that electron itself. The exchange term has the effect of removing charge with the same spin from the vicinity of a charge. This correlation of electrons with the same spin will result in a lower energy for the electron than the case where it is not considered, and is therefore an important feature of the Hartree-Fock method.

For the case of closed shells, it has been shown that the electron spin orbitals must have the form of the solutions of a central field problem (12). That is, the exchange term for a closed shell

must be of the form of a central field. However, this is just the form of the equation encountered in the hydrogen atom which separates into a radial equation including the central field potential, and an equation over angles whose solutions are just spherical harmonics. Thus, the angular part of the spin orbitals will just be spherical harmonics, leaving only the radial equations to be determined. This set of coupled equations is solved by an iterative method called the self consistent field method. A trial set of wave functions and a value for ϵ_i are assumed, the potentials in the last two terms on the left side of Equation 4. 28 are calculated, and the equations are solved numerically for the radial wave functions. This is tried for several values of ϵ_i until one is found which, at a predetermined value of r, matches the slope and magnitude of the radial functions from an outward integration of r, from 0 to this point, to an inward integration of r, from ∞ to this point. These calculated values of the wave functions are then used to recalculate the potentials, and the equations are solved again until the calculated wave functions become consistent.

The calculations by Knox (29) for argon and Dow and Knox (13) for krypton are more complicated than the problem just described, because the configuration of interest contains two unfilled shells. Dow and Knox have followed the standard procedure for dealing with this situation. Again the usual procedure is to neglect the magnetic interactions in the Hamiltonian. The situation where the net spin-orbit

interaction is small compared with the residual Coulomb interaction, and is, therefore, treated in first order perturbation theory, is just the case of Russel-Saunders or L-S coupling. For the first excited multiplet in argon and krypton, where the angular momenta of five p electrons are coupled to the angular momentum of an s electron, the resulting L-S multiplet consists of three ^3P levels and one ^1P level. In L-S coupling the ^3P term is split from the ^1P term by the residual Coulomb interaction, and then the ^3P term is split into three levels by the spin-orbit interaction as shown in Figure 22. It is clear from the partial energy level diagrams for argon and krypton (Figures 10 and 17), that L-S coupling is not a good approximation to the real coupling. In fact, for the case of krypton the spin-orbit splitting of the ^3P levels is almost as large as the splitting due to the residual Coulomb interaction. Even though L-S coupling is not a good description of the coupling in argon and krypton, it is necessary in the Hartree-Fock method, in order to treat the residual Coulomb interaction, to use L-S coupled single particle wave functions. Therefore, for a configuration containing an incomplete shell, a single determinant of one electron wave functions is no longer an adequate approximation to the wave function for the system. Instead, a linear combination of such determinants containing different members of the set of wave functions of the incomplete group is used for each L-S term. In some cases it may even be necessary to include wave functions from

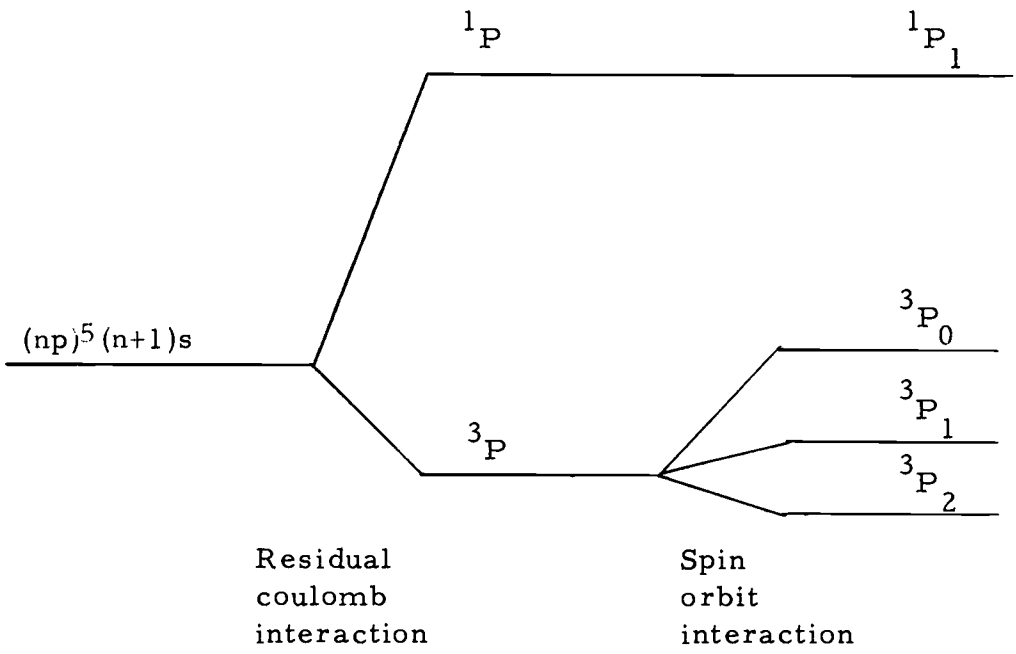

Figure 22. Splitting of energy levels of multiplets for an $(np)^5(n+1)s$ configuration.

other configurations. Furthermore, for incomplete shells it is evident that the potential of an electron in the field of all the others is no longer a central potential. At this point it becomes necessary to make the central field approximation; that is, the potential is assumed to be central. For this approximation the equations separate as before into a radial equation and an equation over angles. The potentials are calculated as before, using only the radial dependence of the wave functions involved. Again the self consistent field method is used until the radial wave functions become self consistent to within the desired accuracy.

As has been mentioned, the anti-symmetrization procedure involved in the calculation just described gives rise to the identification of ^3P and ^1P levels (for the case of interest) with different wave functions and energies. However, the spin-orbit interaction, which is at this point to be included as a perturbation, mixes the $^1P_1$ and $^3P_1$ wave functions. Thus, in order to have a single unperturbed Hamiltonian for the perturbation calculation, the electrostatic exchange terms, which give rise to the energy difference between the triplet and singlet levels, must be identified and treated as part of the perturbation.

The energies and wave functions are then calculated in a straightforward manner using first order perturbation theory. In the partial energy level diagrams for argon and krypton (Figures 10 and

17), the levels are still labeled as pure L-S terms for convenience, even though the spin-orbit interaction has mixed the $^3P_1$ and the $^1P_1$ terms. It is important to keep this in mind, because it is just this mixing which allows a transition from the "$^3P_1$" level to the $^1S_0$ ground state, which is, of course, not allowed in pure L-S coupling. The transition probabilities are then calculated using these mixed wave functions to determine the electric dipole matrix elements for the electrons.

In order to determine the transition probabilities, it is first necessary to calculate a correction to the excited state wave functions (in this case a mixing between the $^3P_1$ level and the $^1P_1$ level) using first order perturbation theory. The calculation of the transition probabilities involves integrals containing the first excited multiplet wave function, correct to the first order, and the ground state wave function. The radial integral involved in this calculation will be small and oscillating and therefore extremely sensitive to small changes in the calculated wave functions. Additionally, since the net spin-orbit interaction in the first excited multiplets of argon and krypton is quite large, it is reasonable to suggest that the inclusion of some configuration mixing will be necessary to bring the calculation into agreement with experiment.

SUGGESTED EQUIPMENT IMPROVEMENTS AND ADDITIONAL EXPERIMENTS

Many improvements have been made on the experimental apparatus, especially during the initial period of development. One improvement, which appears to be both worthwhile and feasible at this time, is to count the output pulses from the photomultiplier instead of detecting an averaged current, as is now done. This would eliminate the noise and drift which are present in the Hewlett Packard Model 425A Electronic Ammeter.

In order to show the possibility of using a pulse counting technique, we must review the present situation. The very small currents which have been encountered in lifetime experiments correspond to the detection of an electron pulse, due to a single photoelectron, about once every million cycles of the excitation of the gas. These pulses are certainly separated enough in time to be counted individually. If the anode was connected to the electrical ground of the system by a short lead through a 50 ohm resistor, each photoelectron would give rise to a 2.7 millivolt anode pulse, assuming that the gain of the photomultiplier is 10^6 and each pulse is a square pulse of 3 nsec duration. Using transistorized electronics, these pulses can be amplified to trigger a digital recorder. However, because of the electronic coupling between the DS02 plate (Refer to Figure 7) and the anode of the photomultiplier, the DS02 gate pulse will induce anode

pulses which are at least as large as the signal pulse. This difficulty could be eliminated by cutting the DS02 plate in a plane parallel to the face of the anode and keeping the section nearer to the anode at -20 volts dc. The remainder of the DS02 plate could still be pulsed as before, but without the large coupling to the anode.

Many worthwhile experiments can be performed with the apparatus as it is now set up. At present, the lifetime for the first excited J = 1 ($^3P_1$) level in argon is being measured again, using the smaller excitation region employed in the krypton experiment. It is hoped that these new data will reduce the uncertainty in the measured value of the $^3P_1$ lifetime.

The lifetimes of the ($2p^5 3s$) $^3P_1$ and $^1P_1$ levels in neon should be measured as an additional check on the calculational procedure developed by Knox. Because of the shorter wave lengths for the resonance transitions in neon, the use of thin films (see page 50) as windows will be necessary. A thin film window will not significantly discriminate against either one of the allowed transitions from the first excited multiplet in neon; therefore, it will be necessary to investigate a two component decay. The calculations by Knox indicate that this may be possible, because the calculated lifetimes for these transitions differ enough that it should be possible to unambiguously resolve the observed decay into two components. The calculated lifetime for the J = 1 ($^3P_1$) level is 20.7 nsec, and that of the J = 1 ($^1P_1$)

level is 2.0 nsec.

It may also be possible to measure the lifetime of the $3p^5 4s$ ($^1P_1$) level in argon by the use of a thin film window. Again, Knox's calculations indicate that this lifetime may be substantially shorter than that of the $^3P_1$ transition, permitting the analysis of the two component decay to be made. It is only after the lifetimes for both the $^1P_1$ and $^3P_1$ levels are known that the mixing of the corresponding Russel-Saunders coupled wave functions can be calculated precisely, thus allowing a much better qualitative criticism of Knox's calculations.

BIBLIOGRAPHY

1. Anderson, D. Kent. Lifetimes of the $(tp^5 6s)\ ^1P_1$ and $^3P_1$ states of xenon. Physical Review 137:A21-A26. 1965.

2. Barrat, J. P. Étudi de la diffusion multiple cohérente de la lumière de résonance optique. Application au niveau $6\ ^3P_1$ du mercure. I. Étude théorique. Le Journal de Physique et le Radiaum 20:541-548. 1959.

3. _____ Étudi de la diffusion multiple cohérente de la lumière de résonance optique. Application au niveau $6\ ^3P_1$ du mercure. II. Étude théorique. Le Journal de Physique et le Radium 20:633-646. 1959.

4. _____ Étudi de la diffusion multiple cohérente de la lumière de résonance optique. Application au niveau $6\ ^3P_1$ du mercure. III. Résultes expérimentaux. Le Journal de Physique et le Radium 20:657-668. 1959.

5. Bennett, R. G. and F. W. Dalby. Experimental determination of the oscillator strength of the first negative bands of N_2^+. The Journal of Chemical Physics 31:434-441. 1959.

6. Bennett, W. R., Jr. and P. J. Kindlmann. Radiative and collision-induced relaxation of the atomic states in the $2p^5 3p$ configuration of neon. Physical Review 149:38-51. 1966.

7. Bickel, William S. and Allan S. Goodman. Mean lives of the 2p and 3p levels in atomic hydrogen. Physical Review 148:1-4. 1966.

8. Breit, G. Quantum theory of dispersion. Parts VI and VII. Reviews of Modern Physics 5:91-140. 1933.

9. Brossel, J. and F. Bitter. A new "Double Resonance" method for investigating atomic energy levels. Application to Hg $^3P_1$. Physical Review 86:308-316. 1952.

10. Compton, K. T. Theory of ionization by cumulative action and the low voltage arc. Physical Review 20:283-299. 1922.

11. Condon, E. U. and G. H. Shortly. The theory of atomic spectra. London, Cambridge University Press, 1951. 441 p.

12. Delbrück, M. The interaction of inert gases. Proceedings of the Royal Society of London, ser. A, 129:686-698. 1930.

13. Dow, John D. and Robert S. Knox. Excited-state wave functions, excitation energies, and oscillator strengths for krypton and xenon. Physical Review 152:50-56. 1966.

14. Duckett, J. W. and P. H. Metzger. Intrinsic photoemissions of alkali halides. Physical Review 137:A953-A957. 1965.

15. D'yakonov, M. I. and V. I. Perel'. Coherence relaxation during diffusion of resonance radiation. Zhurnal eksperimental'noi i teoreticheskoi fiziki 47:1483-1495. 1964. (Translated in Soviet Physics JETP 20:997-1004. 1965.)

16. Garstang, R. H. and Janet Van Blerkom. Transition probabilities in the Ar I spectrum. Journal of the Optical Society of America 55:1054-1057. 1965.

17. Glennon, B. M. and W. L. Wiese. Bibliography on atomic transition probabilities. Washington, D. C., 1962. 42 p. (National Bureau of Standards. Monograph 50)

18. Goodrich, G. W. and W. C. Wiley. Resistance strip magnetic electron multiplier. Review of Scientific Instruments 32:846-849. 1961.

19. Hanle, W. Über magnetische Beeinflussung der Polarisation der Resonanz fluoreszenz. Zeitschrift für Physik 30:93-105. 1924.

20. Harshaw Chemical Company. Synthetic optical crystals. Cleveland, Ohio, 1955. 36 p.

21. Hartree, Douglas R. The calculation of atomic structures. New York, John Wiley and Sons, 1957. 181 p.

22. Hartree, Douglas R. and W. Hartree. Self-consistent field with exchange for potassium and argon. Proceedings of the Royal Society of London, ser. A, 166:450-464. 1938.

23. Heron, S., R. W. P. McWhirter and E. H. Rhoderik. Measurements of lifetimes of excited states of helium atoms. Proceedings of the Royal Society of London, ser. A, 234:565-583. 1956.

24. Heroux, L. and H. E. Hinteregger. Resistance strip magnetic photomultiplier for the extreme ultraviolet. Review of Scientific Instruments 31:280-286. 1960.

25. Holstein, T. Imprisonment of resonance radiation in gases. Physical Review 72:1212-1233. 1947.

26. _____ Imprisonment of resonance radiation in gases. II. Physical Review 83:1159-1168. 1951.

27. Kibble, B. P., G. Copely and L. Krause. Effect of imprisonment of radiation in sodium vapor on the measured lifetime of the $3\ ^2P$ states. Physical Review 153:9-12. 1967.

28. Klose, Jules Z. Atomic lifetimes in neon I. Physical Review 141:181-186. 1966.

29. Knox, Robert S. Excited-state wave functions, excitation energies, and oscillator strengths for argon ($3p^5 4s$). Physical Review 110:375-381. 1958.

30. Lawrence, G. M. and Blair D. Savage. Radiative lifetimes of uv multiplets in boron, carbon, and nitrogen. Physical Review 141: 67-70. 1966.

31. Lincke, R. and H. R. Griem. Method for the determination of atomic-resonance line-oscillator strengths from widths of optically thick emission lines in T-tube plasmas. Physical Review 143:66-73. 1966.

32. Milne, E. A. The diffusion of imprisoned radiation through a gas. Journal of the London Mathematical Society 1:40-51. 1926.

33. Mitchell, Allan C. G. and Mark Zemansky. Resonance radiation and excited atoms. London, Cambridge University Press, 1934. 338 p.

34. Moore, Charlotte. Atomic energy levels. Vol. 1. Washington, D. C., 1949. 309 p. (National Bureau of Standards. Circular 467)

35. _____ Atomic energy levels. Vol. II. Washington, D. C., 1952. 227 p. (National Bureau of Standards. Circular 467)

36. Morack, J. L. and C. E. Fairchild. Measured lifetime of the $(3p^5 4s)\ ^3P_1$ state of argon. Physical Review 163:125-129. 1967.

37. Morse, F. A. and F. Kaufman. Determination of ground-state O, N, and H by light absorption and measurement of oscillator strengths. Physical Review 42:1785-1790. 1965.

38. Prag, A. B., C. E. Fairchild and K. C. Clark. Measured oscillator strengths for the allowed 2p-3s transitions from the ground state in oxygen and nitrogen. Physical Review 137:A1358-A1363. 1965.

39. Slater, John C. Quantum theory of atomic structure. Vol. I. New York, McGraw-Hill Book Company, 1960. 502 p.

40. _____ Quantum theory of atomic structure. Vol. II. New York, McGraw-Hill Book Company, 1960. 439 p.

41. Turner, R. Decay of resonance radiation in a pulsed discharge in krypton. Physical Review 140:A426-A431. 1965.

42. Wilkinson, P. G. Oscillator strenghts of resonance lines of the rare gases--I. Krypton. Journal of Quantum Spectroscopy and Radiative Transfer 5:503-510. 1965.